Early life lipid overload in Native American myopathy is phenocopied by *stac3* knock out in zebrafish

Rajashekar Donaka[1], Houfeng Zheng[2], and David Karasik[1, 3*]

[1]The Musculoskeletal Genetics Laboratory, The Azrieli Faculty of Medicine, Bar-Ilan University, Safed 1311502, Israel

[2]Westlake Laboratory of Life Sciences and Biomedicine, 18 Shilongshan Road, Cloud Town, Xihu District, Zhejiang, 310024, Hangzhou, China

[3]Hebrew SeniorLife, Hinda and Arthur Marcus Institute for Aging Research, Boston, MA 02131, USA

*Corresponding author:

David Karasik, PhD

The Musculoskeletal Genetics Laboratory

Azrieli Faculty of Medicine, Bar-Ilan University, Safed

1311502, Israel

david.karasik@biu.ac.il

Abstract

Understanding the early stages of human congenital myopathies is critical for proposing strategies for improving skeletal muscle performance by the functional integrity of cytoskeleton. SH3 and cysteine-rich domain 3 (Stac3) is a protein involved in nutrient sensing, and is an essential component of the excitation-contraction (EC) coupling machinery for Ca^{2+} releasing. A mutation in *STAC3* causes debilitating Native American myopathy (NAM) in humans, and loss of this gene in mice and zebrafish resulted in death in early life. Previously, NAM patients demonstrated increased lipids in skeletal muscle biopsy. However, elevated neutral lipids could alter muscle function in NAM disease via EC coupling apparatus is yet undiscovered in early development.

Here, using a CRISPR/Cas9 induced *stac3* knockout (KO) zebrafish model, we determined that loss of *stac3* led to muscle weakness, as evidenced by delayed larval hatching. We observed decreased whole-body Ca^{2+} level at 5 days post-fertilization (dpf) and defects in the skeletal muscle cytoskeleton, i.e., F-actin and slow muscle fibers at 5 and 7 dpf. Homozygous larvae exhibited elevated neutral lipid levels at 5 dpf, which persisted beyond 7 dpf. Myogenesis regulators such as *myoD* and *myf5*, were significantly altered in *stac3*$^{-/-}$ larvae at 5 dpf, thus a progressive death of the KO larva by 11 dpf.

In summary, the presented findings suggest that *stac3*$^{-/-}$ can serve as a non-mammalian model to identify lipid-lowering molecules for refining muscle function in NAM patients.

Keywords: Native American myopathy, zebrafish, cytoskeleton of muscle, muscle weakness, neutral lipids.

Introduction

The musculoskeletal system provides a unique framework for bone, skeletal muscle, and connective tissue for enabling mobility and withstanding mechanical load generated in daily activities of human life. Skeletal muscle (~40% in the human body mass) serves to provide anatomical support for the bones/internal organs, to produce contractions and to store energy for locomotion, all essential structures and processes for the survival of an organism[1]. Defects in the genetic makeup or metabolic activity of skeletal muscle result in dystrophy, myopathy, cachexia and/or sarcopenia. Among these muscle diseases, myopathies have often been reported as heterogeneous entities that include channelopathies, inflammatory, metabolic, mitochondrial, and myotoxic diseases, which affect 1.62 in 100,000 individuals of all ages across the globe[2, 3, 4, 5].

Muscle weakness is one of the key hallmarks of congenital myopathies (1 in 26,000)[6], while its further consequences are escalated fibrosis, fat infiltration, and degenerating myofibers[7]. The cytoskeleton of muscle tissue is composed of filamentous actin (F-actin) and myosin. Of late, it was shown that the structural position of fast muscle cell fusion was guided by slow muscle fibers in myotome formation[8]. In vertebrates, slow muscle fibers originate from somitic mesoderm as one of the embryonic lineages; these embryonic lineages further differentiate into the first muscle fiber types to perform longer contractions by firing action potential[8, 9, 10]. In early life, human myopathies are usually associated with accumulation of disorganized actin, α-actinin and myosin, and failure of myofibrillar assembly in fast-twitch muscle fibers[11].

Historically, Native American myopathy (NAM) was identified in the Lumbee Indian infant population of North Carolina, USA. The genetic predisposition to NAM was determined to be caused by homozygosity for a variant G>C in exon 10 of *STAC3*, a gene highly expressed in skeletal muscle. The STAC3 protein contains a Src homology 3 (SH3) and cysteine-rich C1 domains. Clinically, other genetic mutations in *STAC3* result in congenital anomalies, such as

cleft palate, micrognathia, *talipes equinus* (club foot), and arthrogryposis also found in NAM patients. Besides these skeletal abnormalities, NAM patients demonstrate increased levels of neutral lipids in muscle biopsy and it was reported that one-third of patients (36%) of disease afflicted individuals die before the age of 18 years[12, 13]. Of late, it was suggested that C1 domain of STAC3 is likely to bind the lipids[14]. Multiple studies have focused on investigating the regulation of *STAC3* in NAM. Among all, *Stac3* knockout mice had a higher percentage of type I (oxidative) muscle fibers and exhibited poor musculoskeletal performance[15]. Transcriptional regulation of *Stac3* suggests that nutrient balance is a prerequisite for cytoskeletal integrity and myogenesis via energy metabolism[16]. However, the genetic etiology and pathophysiology of slow skeletal muscle weakness in NAM remain largely elusive.

Conventionally, lipids play a significant role in energy homeostasis, cellular structure and cellular signaling, while lipid composition is crucial for ion channel activity and maintenance of membrane receptor conformation[17, 18]. Oftentimes, alterations in lipid metabolism account for metabolic muscle diseases[19]. Importantly, storage of complex lipid molecules or glycogen content in skeletal muscle can modify the calcium (Ca^{2+}) release at excitation-contraction (EC) coupling apparatus on sarcoplasmic reticulum (SR). Interestingly, calcium-sensing dihydropyridine receptor (DHPR) and calcium-releasing ryanodine receptor (RYR1) are under the control of STAC3 for intracellular functions including muscle contractions[20, 21]. These physiological actions involving the EC apparatus underscore the absolute necessity of STAC3 for Ca^{2+} and nutrients homeostasis.

One decade ago, the first *stac3* knockout study in zebrafish revealed that a mutation in the *stac3* gene of zebrafish (ZF) larvae impeded muscle function through EC coupling-driven defects in the motor system in early life. STAC3 regulates the amount and stability of DHPR and/or RYR1 at skeletal muscle triads by protein trafficking[22]. Markedly, the nutrient load (neutral lipids) accelerates degeneration of filamentous actin (F-actin) and slow muscle myosin (Smyhc1) fibers,

which exemplify harmful behaviour of lipids in the maturation of skeletal muscle fibers. Thus, identification of genetically-driven metabolic peculiarities, i.e., in lipid composition, may be vital for preventing the loss of muscle fibers. Such disease-associated fatty acids may serve as biomarkers for the early diagnosis of the disease or primary clinical indicators of treatment success of NAM patients.

Of late, human myopathies have been modeled by knocking-out disease-causing genes using CRISPR/Cas9 technology. In parallel, ZF serve as remarkable teleost animal model for skeletal muscle research[23] and as a non-mammalian model for myopathies. Inherently, ZF acquired multiple advantages, including high fecundity, external fertilization, and quick transformation of one-to-multiple somite stages of the larva, which could provide substantial clinical and histopathological information on the muscle disease[24, 25]. The current study generated *stac3*$^{-/-}$ zebrafish using CRISPR/Cas9 technology. Remarkably, the *stac3*$^{-/-}$ fish resemble human phenotypes of Native American myopathy with increased neutral lipids level in the larvae. This metabolic disbalance was further evident in structural and functional defects in zebrafish, which seemingly drive failure of *stac3*$^{-/-}$ larvae's musculature and their early demise.

Methods

Animal husbandry

Danio rerio zebrafish strains were maintained at 28 °C, under a 14:10 light: dark cycle and their offspring was propagated until 6 dpf in system water containing 0.1% methylene blue (embryo water) and then transferred to the system (nursery) or kept in the Petri dishes sans methylene blue, for beginning of feeding. All animal experiments were conducted in accordance with the Faculty of Medicine's Zebrafish Facility, Bar-Ilan University, Israel, Institutional Animal Care and Ethical Committee (IACUC) guidelines. The protocol was approved by the committee (protocol #53-08-2020).

Generation of *stac3*$^{-/-}$ by CRISPR/Cas9 system

The strategy for establishing a stable zebrafish knockout followed a published CRISPR/Cas9 protocol[26]. In brief, the guide RNA (gRNA) was designed to target sequence 5'-AGTTCTGTGACGTCTGCGCACGG- 3' in exon 4 of the *stac3* gene. The *FspI* restriction enzyme (New England BioLabs, Cat#R0135S) was utilized to distinguish between mutant, wild type and heterozygous fish (Supplementary materials and methods). At the one-cell stage (30-45 minutes post-fertilization), wild type zebrafish embryos of AB strain (F0) were injected with a mixture of gRNA, crRNA, tracer RNA and Cas9 protein (Abcam, Cat#224892), at total amount of 300 µg/µL, using a pneumatic Pico Pump (WPI, Worcester, MA, USA), and embryos were transferred into the incubator.

Genotyping and sequencing

After 24 hours, DNA was extracted from of subset of pooled gRNA mix-injected embryos. A polymerase chain reaction (PCR) was carried with forward primer: 5'-GTGTTTTCAACGTTAGTTCTGCTG-3' and reverse primer: 5'-TGGCAAGAACAGTTTACCTTAACA-3'. The reactions were performed using two programs: (A) DNA was denatured at 94 °C for 3 seconds, annealed at 63 °C for 3 seconds and extended at 72 °C for 5 cycles, 3 seconds each. (B) DNA was denatured at 94 °C for 3 seconds, annealed at 60 °C for 3 seconds and extended at 72 °C for 37 cycles, 3 seconds each, followed by final extension at 72 °C, for 3 minutes. Products of PCR amplification and restriction digestion were examined on a 2% agarose gel. The 10-base-pair (bp) deletion was verified by DNA sequencing (Hy-lab, Rehovot, Israel and Macrogen, Amsterdam, Netherlands).

For generation of a stable knockout, CRISPR/Cas9-targeted larvae were grown in a 1-liter (L) tank for 35 days and then maintained in 3-L tank in a system water. At 2 months post-fertilization (mpf), fish were genotyped to identify a founder that carried a mutation. Germline transmission of a mutation in F1-progeny was deciphered by crossing the adult founders (F0) to WT. To acquire

the 10 bp deletion in F2-progeny, adults (F1) were out-crossed to WT. To minimize an off-target effect, adult fish carrying the 10 bp deletion (F2) were further outcrossed to WT. The *stac3*$^{+/+}$, *stac3*$^{+/-}$, and *stac3*$^{-/-}$ siblings were obtained by intercrossing *stac3*$^{+/-}$ F3 adult parents.

Calculating hatching percentage of *stac3*$^{-/-}$ zebrafish larvae

Mass spawning of adult *stac3*$^{+/-}$ parents produced all three genotypes: *stac3*$^{+/+}$, *stac3*$^{+/-}$ and *stac3*$^{-/-}$ according to the Mendelian ratio. After spawning, embryos were collected and grown in a Petri plate containing embryo water. During the course of somite to muscle fiber transition, the number of hatched and unhatched larvae was recorded at 3, 4 and 5 dpf, and delayed hatching of the larvae was documented by bright field light microscope imaging, while their genotypes were verified by DNA sequencing of pooled sample (n=10) for each group. Delayed hatching observations and analyses were conducted on at least three independent clutches of parent's spawning. We saw skeletal peculiarities early on, thus we identified larvae as "normal" (*stac3* wild type and heterozygous siblings) and "deformed" (*stac3* knockout) for the ensuing study.

As a rule, larvae were examined under the light microscope every 24 hours. The total number of embryos produced by *stac3*$^{+/-}$ parents was recorded. Dead larvae at (4-11 dpf) were extracted from Petri plates and genotyped. In all experiments, larvae were euthanized in 0.4% methane sulfonate (Sigma-Aldrich, MS-222) with subsequent immersion in ice-cold water for 15 minutes.

Whole-body Ca^{2+} measurement during larval development

Total body calcium level was determined for zebrafish larvae groups, i.e. *stac3*$^{+/+}$ and *stac3*$^{+/-}$: n=90 and *stac3*$^{-/-}$: n=60). After euthanasia, larvae were washed gently with deionized water and dried for 1 hour at 65 °C. Then, samples were digested with 80-90 µL 1M Tris-Cl (pH 8.0), at 95 °C, overnight. Digested samples were centrifuged at 13,000 rpm for 5 minutes and the supernatant was collected in 1.5 mL Eppendorf tube. Calcium amount was detected using the Colorimetric Calcium Assay Kit (Abcam, Cat#102505), according to the manufacturer's

instructions. Optical density of each sample was measured at 575 nm with absorption spectrometry (Tecan-Plate Reader-Spark Cyto, DKSH technology, Bangkok, Thailand).

RNA extraction

We extracted RNA from *stac3* wild type and heterozygous siblings and *stac3* knockout for gene expression analysis at 4 and 5 dpf. After euthanasia, pooled (n=10) larvae were homogenized with a pestle and motor mixer (Thomas Scientific, Swedesboro, NJ, USA, Cat#47747-370) in 350 µL Trizol (Sigma-Aldrich). RNA was extracted in biological triplicates, using the Direct-Zol RNA kit (Zymo Research, Tustin, CA, USA).

Real-time quantitative PCR (RT-qPCR)

cDNA (500-1000 ng) was synthesized using the Takara PrimeScript Kit (Takara, Mountain View, CA, USA). Gene expression was quantified using the PowerUp SYBR Green Master Mix and a ViiA™7 Dx qPCR Instrument (Thermo Fisher Scientific, Waltham, MA, USA, Cat#4453534). The target gene expression (TableS1) was normalized to the endogenous control *rpl32* (ribosomal protein l32). For each expression analysis, a non-template control (NTC) was included along with technical triplicates. Delta-delta-threshold cycle (DDCT) values were plotted on the graph as relative gene expression.

Whole-mount staining of zebrafish larvae

At 5 and 7 dpf, *stac3*$^{+/+}$ and *stac3*$^{+/-}$: n=15 and *stac3*$^{-/-}$: n=15 larvae were fixed in 4% paraformaldehyde (PFA, Sigma-Aldrich) either for 1 hour at RT or overnight at 4 °C. Staining was performed using a published protocol[27]. Slow muscle fibers were stained with the anti-Myhc (F59, Santa Cruz Biotechnology, Dallas, TX, USA, Cat#sc-32732) antibody (1:1000 dilution). F-actin fibers were stained with Phalloidin (iFluor 488, Cat#Ab176753) (1:1000 dilution), followed by secondary antibody (Sigma-Aldrich).

Neutral lipid visualization by Oil Red O (ORO) staining

ORO (Sigma Aldrich, Cat#0-0625) powder 0.05 g was dissolved in 10 mL isopropanol and then incubated for 10 minutes at RT. The ORO working solution was prepared by adding three parts of filtered ORO stock to the two parts of distilled water. Muscle section-containing slides were air-dried for 2-3 hours at RT, washed with 1x PBS for 2 minutes and air-dried again for 2-3 hours. The slides were incubated in 500 µL ORO working solution for 30 seconds, then washed with tap water and air-dried for another 3 hours at RT, before mounting them in 100% glycerol.

Muscle histology

Embedding of zebrafish larva

At 5 dpf, larvae were fixed in 4% PFA for 3-6 days, at 4 °C, and washed 3x with PBS for 15 minutes. Then, they were soaked in 10% sucrose for 48 hours at RT, and then embedded with Tissue Tek (Sakura, Torrance, CA, USA) in 12x12 cm embedding molds (PEEL-A-WAY; Cat#70181). The embedding molds were frozen in liquid nitrogen for about 2-3 hours, and then stored in aluminum foil, at -20 °C. Muscle sections were cut serially to 20 µM thickness with a cryostat (Leica CM1950), and sections were collected on 26X76 mm/1-1.2 mm adhesion microscope slides (BAR-NAOR Ltd., Tel Aviv, Israel, Cat#BN93080C).

Hematoxylin and eosin staining

Paraffin-based horizontal muscle sections were dehydrated 3x in xylene for 2 minutes, and then dehydrated in 100% alcohol, before being washed with 80% alcohol and tap water. Slides were then stained with both hematoxylin and eosin solution using the LEICA AUTOSTAINER XL at the Department of the Pathology, Ziv Hospital, Safed, Israel.

Locomotion of *stac3*$^{-/-}$ larvae

To quantify locomotion function of *stac3* KO, *stac3*$^{+/+}$ and *stac3*$^{+/-}$ (n=48) and *stac3*$^{-/-}$ (n=22) larvae were grouped at 5 dpf. Tracking was performed with a DanioVision system (Noldus Information technology, Wageningen, NL). For habituation, larvae were individually placed before the test, in

96-well-plates containing 200 µL embryo water (A1-D12: *stac3*$^{+/+}$ and *stac3*$^{+/-}$ and E1-F10: *stac3*$^{-/-}$) and incubated for 30 minutes at 28 °C. The locomotion tracking strategy included 15 minutes light on, 5 minutes light off, 5 minutes light on. Total distance moved by larvae was averaged for every one-minute represented by a dot on the graph under each (light/dark) condition. After the test, larvae genotype was confirmed using the *FSPI* enzyme digestion.

Senescence-associated (SA) β-galactosidase staining

To assess the effect of senescence on early life muscle fiber growth and development in zebrafish, larvae at 6 dpf were classified as normal or deformed and fixed in 4% PFA, at 4 °C, overnight. Larvae were washed with phosphate buffered saline (PBS pH 7.4, followed by PBS pH 6.0), 3x for 10 minutes each. Next, larvae were incubated with 1% X-Gal solution [in PBS pH 6.0: 1 mg of 5-bromo-4-chloro-3-indolyl beta-D-galactosidase (X-Gal)] per mL, 5 mM $K_3Fe[CN]_6$, 5 mM $K_4Fe[CN]_6$,150 mM NaCl and 2 mM $MgCl_2$ (Sigma-Aldrich) at 37 °C, overnight[28]. Images were acquired with a bright field microscope.

Skeletal muscle defects observed by birefringence assay in zebrafish larvae

stac3$^{+/+}$ and *stac3*$^{+/-}$ control siblings and *stac3*$^{-/-}$ larvae were anesthetized on 6 dpf and positioned to allow a dorso-ventral view, in 3% methylcellulose. Muscle fiber architecture was assessed, as described in the published protocol[29] at the Faculty of Marine Sciences, Ruppin Academic Center, Mikhmoret, Israel.

Caffeine treatment of zebrafish larvae

At 5 and 7 dpf, *stac3*$^{+/+}$ and *stac3*$^{+/-}$ control siblings and *stac3*$^{-/-}$ larvae (sample sizes from 25 to 30 animals per group), were subjected to caffeine treatment (Sigma-Aldrich, Cat#C0750). Stock caffeine 1M solution was prepared in double distilled water, and a working concentration of 5mM caffeine (v/v) was subsequently diluted in 1L system water. Each petri dish contained either 30mL of working solution of caffeine or embryo water as no-treatment control solution. Survival of the

larvae was monitored for 4 days (96 hours), and each day dead larvae were visually recorded by using the light microscope (then discarded).

Image processing

Embryo hatching, developmental defects, and whole-mount Oil Red O staining of neutral lipids were imaged using a Leica microscope (M165 FC). Muscle histology imaging was performed with an automated upright slide-scanning microscope (Axio Scan.Z1, Carl Zeiss Microscopy, Oberkochen, Germany) with a 20×/0.95 objective at z-planes of 0.5mm. Fluorescent images were taken with upright microscope (Apotom.2, Carl Zeiss, Jena, Germany).

Data analysis

Most of the experimental data were analyzed with Prism (version 9, GraphPad Software, Inc., La Jolla, CA, USA) and some data sets were processed in Excel. All graphs present means ± standard deviation values. Two independent groups were compared using the student's t-test. Larvae locomotor activity was analyzed by one-way ANOVA. Survival rate of knockout fish was determined by Prism, using the Log-rank test. In all the analyses, statistical significance was defined as a $p<0.05$.

Results

1. Generation of CRISPR/Cas9 based *stac3* knockout line in zebrafish to study NAM disease process

Loss of *STAC3* leads to severe skeletal abnormalities in both mice and zebrafish, although a mechanism by which *stac3* mutants die at an early age[22, 15] is unknown. Further, morbidity in NAM patients had associated with increased lipid levels in skeletal muscle. To study the relation between early muscle fibers development and lipid metabolism, CRISPR/Cas9 system was applied to induce a global knockout of exon 4 of *stac3*. A 10-base-pair deletion in ZF was generated, which led to a frame shift which created a stop codon at V78 and produced a truncated

protein (80 aa total length) (Fig1A, B). The targeted knockout in *stac3* gene was confirmed by both *FspI* restriction enzyme digestion and sequencing of genomic DNA (Fig1C and FigS1A, B). Adult *stac3* heterozygous (*stac3*$^{+/-}$) parents were then inter-crossed to obtain homozygous (knockout) *stac3*$^{-/-}$ offspring. Further, *stac3*$^{+/-}$ progeny were "blindly" characterized as we saw congruence with skeletal phenotypes at the early development of the homozygous larvae. ZF larvae from 2-3 independent clutches were then selected based on their morphology, - either normal (healthy; *stac3*$^{+/+}$ and *stac3*$^{+/-}$) or deformed (*stac3*$^{-/-}$) - for functional characterization of skeletal muscle tissue at the early life. All unhatched larvae were genotypically confirmed as *stac3* knockouts (FigS2A-C). At 3 days post-fertilization (dpf), *stac3*$^{-/-}$ larvae exhibited multiple congenital skeletal muscle defects, such as bending at head, trunk, and tail regions, and were distinct from *stac3*$^{+/+}$ and *stac3*$^{+/-}$ control siblings (FigS1C). RT-qPCR analysis showed that the relative gene expression of *stac3* was significantly ($p<0.05$) downregulated in knockout compared to *stac3*$^{+/+}$ and *stac3*$^{+/-}$ control siblings at 5 dpf (Fig1D). These findings align with previous observations in *stac3* mutant mice and ZF; we therefore utilized *stac3*$^{-/-}$ zebrafish for identifying genetically-driven metabolic regulators, which could be potentially associated with human muscle disease (congenital myopathies) pathology.

2. *stac3* knockout constrains embryo hatching by altered Ca^{2+} level via *ryr1a* receptor in zebrafish

The *Stac3* gene plays a vital role in calcium homeostasis by modulating calcium-sensing dihydropyridine (DHPR) receptor and calcium-releasing ryanodine (RYR1) receptor at the sarcoplasmic reticulum[20]. We presumed that a mutation in *stac3* gene causes muscle weakness by altering physiological calcium level in zebrafish at early life. Intercrosses of adult *stac3*$^{+/-}$ parents produced all three genotypes: *stac3*$^{+/+}$, *stac3*$^{+/-}$ and *stac3*$^{-/-}$ larvae; the proportion of these genotypes complied with the Mendelian ratio. On 4 dpf, there was a significant ($p<0.05$) delay in hatching of stac3 knockout larvae (12%) compared to wild type and heterozygous control siblings

289 (76.7%) (Fig2A, B). Under physiological conditions, muscle function (contraction) begins at 17
290 hours post-fertilization in ZF, such that, by 2 dpf, larvae are completely shed their chorion through
291 rapid contractions[22]. Therefore, we sought to determine whether mutation in *stac3* alters lipid
292 metabolism, resulting in damage to muscle fiber functional organization, consequently promoting
293 the early death of ZF larvae.
294 Indeed, we found that *stac3*$^{-/-}$ larvae carrying 10 bp deletion mutation died within the chorion at 4
295 dpf, which was not seen in their controls siblings (FigS2A), suggesting that severity of declined
296 muscle function (muscle weakness) gradually escalated. Moreover, genotypes of hatched and
297 unhatched larvae were verified by DNA sequencing of a pooled sample (n=10) from each group
298 (FigS2B, C). To determine whether low Ca^{2+} constrain hatching of ZF larvae, the progeny of
299 *stac3*$^{+/-}$ parents was categorized into contrasting phenotypic groups for measuring whole body
300 Ca^{2+} levels. Whole-body Ca^{2+} levels were compared between hatched vs. unhatched and normal
301 vs. deformed larvae. As anticipated, total-body calcium levels were significantly lower ($p < 0.05$;
302 Fig2C) in *stac3* knockout in comparison to *stac3*$^{+/+}$ and *stac3*$^{+/-}$ (control) siblings at the early
303 muscle fibers growth and development. In parallel, we found that the relative gene expression of
304 ryanodine receptor 1a (*ryr1a*) was significantly ($p=0.0171$; Fig2D) elevated in *stac3*$^{-/-}$ larvae
305 compared to their controls. These results suggest that a mutation in *stac3* leads to a calcium
306 deficiency via *ryr1a* receptor, which impedes skeletal muscle function, as demonstrated by
307 delayed embryo hatching and declined locomotion (Fig7A, B and Fig9).

308 **3. F-actin inadequacy and slow muscle fiber organization in *stac3*$^{-/-}$ larvae**

309 stac3 knockdown has been shown to affect myofibrillar protein assembly[16]; we sought to
310 determine whether *stac3* knockout can affect the cytoskeleton of skeletal muscle i.e., F-actin and
311 slow myosin wirings. In humans, BA-D5 antibody was known to recognize one of the myosin MHC
312 (cardiac β) isoforms[30]. Therefore, we performed slow muscle (anti-Myhc; F59) staining for
313 visualization of all myosin isoforms in knockout *stac3*, heterozygous and wild type siblings at the

age of 5 and 7 dpf. Consequently, disorganized slow muscle fibers and a deficit in conventional organization of individual fibers were identified in trunk and tail regions of *stac3*$^{-/-}$ larvae compared to *stac3*$^{+/+}$ and *stac3*$^{+/-}$ siblings at 5 dpf, this was more prominent with larger gaps at somite boundaries at 7 dpf (Fig3A-C and FigS3A and FigS4A, C panel). Furthermore, whole-body F-actin fibers were reduced in the *stac3* KO in contrast to *stac3*$^{+/+}$ and *stac3*$^{+/-}$ siblings (Fig3D and FigS3B). The myosin structural organization is essential for energy production of skeletal muscle for contractions[31]. In comparison to *stac3*$^{+/+}$ and *stac3*$^{+/-}$ control siblings, *stac3*$^{-/-}$ larvae showed a significant reduction in relative expression of both *srebf1* (p=0.0025) and its down-stream target acetyl co-enzyme-A (p=0.004), that are involved in lipogenesis (FigS3D). Therefore altered cytoskeleton architecture of skeletal muscle could impair metabolic processing of nutrients (lipids) in *stac3* KO.

4. Expression of myogenic regulators is dysregulated in *stac3*$^{-/-}$ larva

STAC3 is highly expressed in skeletal muscle tissue. Therefore, we sought to check whether the fragility of the musculoskeletal system in early life of the *stac3*$^{-/-}$ is dictated by impaired myogenesis, relative gene expression of myogenesis markers was evaluated. The lineage of skeletal muscle in the embryonic stage is determined by myogenic regulatory factors such as *MYOD*, *MYF5*, and *MYOG*[32]. Similarly, RT-qPCR analyses identified significant upregulation of *myoD* (p=0.001) alongside downregulation of *myf5* (p=0.03) and unaltered expression of *myoG* in *stac3*$^{-/-}$ larvae as compared to wild type and heterozygous controls at 5 dpf (Fig4A-C). Genetically, *MYOD* and *MYF5* are *bona fide* for myoblast fusion by maintaining the functional organization of actin and myosin fibers, while *MYOG* involves in the terminal differentiation of muscle cells[33]. Disorganized slow muscle fibers with a reduced amount of F-actin were found at 5 and 7 dpf in *stac3*$^{-/-}$ larvae (Fig3). However, gene expression of skeletal muscle markers such as *sox6*, slow muscle myosin (*smyhc1*), and troponin (*tnnca1*) were unchanged in *stac3*$^{-/-}$ compared to the *stac3*$^{+/+}$ and *stac3*$^{+/-}$ groups at 5 dpf (FigS3C). To our notice, it was shown that

MyoD$^{-/-}$ mice are viable and fertile while contrastingly double knockout of *MyoD* and *Myf5* had led to a perinatal death[34]. Further, we show that unaltered *myoG* expression of *stac3*$^{-/-}$ larvae indicates defective signals that could commence in myogenesis before the formation of complete skeletal muscle fiber (Fig4D). Furthermore, abnormal histopathological features and compromised myogenesis were reported in myopathies[35]. Altogether, our results suggest that both *myf5* and *myoD* might have compensatory mechanisms of action in *stac3*$^{-/-}$ larvae, to secure cytoskeleton integrity by actin and myosin fibers formation.

5. Distinct lipid metabolism in *stac3*$^{-/-}$ fish at the early life

Besides in adipose and liver tissues, excess neutral lipids are often stored in skeletal muscle tissue, a hallmark of lipid storage myopathy. An increase in lipid droplets was revealed by electron microscope analysis of NAM patient skeletal tissue samples[12, 14]. Therefore, we sought to determine whether lipid metabolism is altered in *stac3*$^{-/-}$ zebrafish and associated with impaired muscle fiber functional organization. At multiple developmental stages, *stac3* knockout and wild type and heterozygous siblings were stained with Oil Red O dye (ORO) for lipid visualization. In early life, zebrafish larvae utilize transported maternal lipids as the energy source for their active metabolic functions[36, 37]. Correspondingly, no differences in whole-body lipids of hatched (*stac3*$^{+/+}$ and *stac3*$^{+/-}$) compared to unhatched (*stac3*$^{-/-}$) larvae were observed on 4 dpf (Fig5A-A'). Notably, elevated neutral lipids were primarily observed in the yolk sac region of knockout larvae compared to *stac3*$^{+/+}$ and *stac3*$^{+/-}$ control siblings (p=0.0023; Fig5B-B' and E) at 5 dpf, which corroborates the increase in lipid droplets measured in NAM patients[12, 38]. Impairments in genetic and metabolic process can affect lipid synthesis, transportation, utilization, and degradation in multiple cell and tissue types, and including skeletal muscle. We therefore further visualized neutral lipids of larvae by whole-mount ORO staining on the day of exogenous feeding (7 dpf) and, in knockout larva, found levels identical to those shown at 5 dpf (Fig5B-B' and Fig5C-C', D), suggesting that *stac3*$^{-/-}$ maintained surplus lipids, while in control groups these levels go down (FigS4B-B'). Of note,

studies[16] reported that *stac3* is involved in nutrition sensing, while its C1 domain binds to lipids[14]. Hence, we speculate that in presence of the *stac3* genetic background wild type and heterozygous siblings are capable of sensing nutrients for generating energy for performing enhanced muscle contractions, and survival of the larva (Fig7A, B and Fig9).

6. Metabolic dysfunction promotes death of *stac3* KO fish

The impact of accumulated lipids in NAM and pathophysiology of skeletal muscle tissue affected by this disease are unknown. However, detrimental effects on cytoskeletal elements and on their interactions in muscle tissue can lead to myopathies in humans[39]. We next asked whether a delay in embryo hatching, reduction in F-actin and alteration in slow muscle fibers organization weaken musculoskeletal system in *stac3* knockout. To confirm whether 10bp deletion mutation alters the structural integrity of *stac3*$^{-/-}$ skeletal muscle, birefringence analysis of *stac3*$^{-/-}$ found a patchy pattern of muscle fibers with dense black spots, whereas *stac3*$^{+/+}$ and *stac3*$^{+/-}$ control siblings had rich on muscle fibers with bright chevron structure on 6 dpf (Fig6A and TableS3). In this study, knockout larvae died gradually by 5 dpf, with obvious skeletal muscle defects; out of the expected by Mendelian ratio for *stac3* knockouts (25%) we found only ~18.24% of knockout larvae survived until 7 dpf (TableS2). To understand the significance of genetic regulation of *stac3* in nutrients processing and its contribution to survival of zebrafish, we further maintained these surviving knockout larvae in an incubator and changed embryo water after feeding with nursery food, suggesting that *stac3* KO carries a systemic metabolic dysfunction manifested by increased neutral lipids (Fig5B, C panels). To determine whether high neutral lipid (nutrients load) levels can induce lethal lipotoxicity in *stac3* knockouts, we performed cellular senescence assay at the early development of zebrafish larvae[28]. As expected, our senescence-associated beta-gal probe (SA-β-gal) was strongly noticeable at the yolk sac region of the *stac3*$^{-/-}$ compared to *stac3*$^{+/+}$ and *stac3*$^{+/-}$ control siblings at 6 dpf (Fig6B, C and FigS5B, C panels). Furthermore, fasting of *stac3* KO larvae revealed a trend of improved survival between 7 and 10 dpf ($p<0.0001$; FigS6). These

findings align with the lipid (ORO) staining observations and suggest that deletion of 10 bp in the *stac3* gene accelerates an early-age-specific senescence in cells, culminating in metabolic failure of the zebrafish larva ($p<0.0001$; Fig6D).

7. Caffeine treatment improves survival of the *stac3*$^{-/-}$ larvae at 5 but not 7 dpf

We sought to determine whether caffeine could be an effective therapeutic molecule to a betterment of congenital myopathies due to its key mechanistic biochemical actions across muscle and other tissues[40]. Previous studies revealed that caffeine treatment had significantly enhanced muscle power with the improvement of Ca^{2+} release, increased fatty acid utilization, and decrease in the mortality of mice by antioxidant functions in brain[20, 41, 42]. We monitored the growth and survival of *stac3*$^{+/+}$ and *stac3*$^{+/-}$ (non-deformed) control siblings and *stac3*$^{-/-}$ larvae with and without 5mM caffeine treatment at two different time points. After 5mM caffeine treatment for 96 hours, we discovered an improvement in the survival of the *stac3*$^{-/-}$ larvae compared to untreated *stac3*$^{-/-}$ control group at 5 dpf (Fig8A). Moreover, the difference of overall survival of the *stac3*$^{+/+}$ and *stac3*$^{+/-}$ control siblings was significantly ($p<0.0001$) increased compared to untreated and treated deformed animals 5 dpf. In the *stac3*$^{-/-}$ zebrafish larvae at 7 dpf, we found that over 96 hours the *stac3*$^{-/-}$ larvae were dying much faster ($p<0.0001$) than their untreated *stac3*$^{-/-}$ and non-deformed control siblings (Fig8B). In contrast to 5 dpf, at 7 dpf deformed larvae did not show any improvement in their survival percentage after 5mM caffeine treatment compared untreated *stac3*$^{-/-}$ (deformed) and treated *stac3*$^{+/+}$ and *stac3*$^{+/-}$ animals. In summary, the mechanistic regulation of *stac3* by caffeine is important during muscle fibers' development at the early life (5 dpf), while caffeine regulation could be inhibited at the start of external feeding - in 7 dpf *stac3*$^{-/-}$ zebrafish.

Discussion

In CRISPR/Cas9-generated *stac3* zebrafish mutants, we noticed that out of the expected Mendelian ratio of 25% only 18.24% *stac3* KO larvae survived till the age of 11 dpf. Additionally, functional and morphological observations of *stac3*$^{-/-}$ larvae suggested muscle paralysis and skeletal muscle deterioration in the early life of *stac3*$^{-/-}$. The present study thus explored the phenotypic basis for early life mortality of *stac3*$^{-/-}$ zebrafish and found that *stac3* is critical for early life lipid balance in ZF. Knocking-out this gene in zebrafish led to a delay in embryo hatching and to skeletal muscle defects, and eventually, to a gradual decline in survival at age 4-11 dpf. Under physiological conditions, muscle function (contraction) begins at 17 hours post-fertilization in ZF, such that, by 2 dpf, larvae should completely shed their chorion through rapid contractions. Of note, a proportion of *stac3*$^{-/-}$ larvae died within the chorion (~4 dpf), which is implying the existence of a paralyzed muscle function during early development. In CRISPR/Cas9 system-induced global knockout, we saw gross phenotypes early on, thus we identified larvae as normal (*stac3* wild type and heterozygous siblings) and deformed (*stac3* knockout) in the entire study. Earlier studies found altered ratios of slow and fast muscle fibers in *Stac3* KO mice, possibly reflecting impaired muscle metabolism[15, 43]. Zebrafish carrying a missense mutation of the *stac3* gene were shown to have EC coupling alteration-instigated swimming impairments, which preceded larval death[22].

To improve the survival of the larvae beyond the age of 11 dpf, we applied special conditions (i.e. nursery feeding and replenishing with a fresh system water) to these 18.24% *stac3* KO larvae that survived, along with *stac3*$^{+/+}$ and *stac3*$^{+/-}$ control siblings. We thus discovered that between 7-11 dpf, expedited mortality was observed in *stac3*$^{-/-}$ fish only. Furthermore, fasting revealed a trend in better survival of fasted vs. fed *stac3* KO larvae between 7 and 10 dpf (FigS6). It could be that nutrient-dependent transcriptional regulation in *stac3* KO zebrafish failed in coping with exogenous feeding. We further sought to measure the expression of myogenic regulators and

lipogenesis synthesis genes to correlate with metabolic activities involved in developing muscle fiber architecture. We found that loss of *stac3* significantly upregulated *myoD* and downregulated *myf5* expression, while *myoG* gene expression was unaltered, whereas *srebf1* and acetyl co-enzyme were significantly down-regulated, which suggests that myogenesis can be independently controlled by *myoD* and *myf5* genes[44, 45]. Congruently, *myoG* mutant larvae showed no effect on muscle phenotypes[45]. Of note, in chicken development, distinct diet conditions associated with increased mRNA levels of myogenic regulators (*Myf5*, *MyoD*, and *Myf4*) controlled the growth of skeletal muscle[46, 47, 48]. Recently, the expression of *MYF5* was reported to be significantly altered in human congenital myopathy[49]. In sum, transcription of the myogenic regulatory factors *myoD* and *myf5*, which encode proteins critical for fine-tuning of musculoskeletal health in zebrafish, is dependent on *stac3*.

In humans, clinical features of congenital myopathies include muscle weakness, increased intramuscular fat and muscle fiber degeneration[50]. Histologically and molecularly, congenital myopathies are categorized into sub-entities based on the affected protein (e.g. desmin, dystrophin, collagen) and lipid contents in skeletal muscle tissue[51, 52, 53]. Of note, NAM patients demonstrate muscle weakness and increased lipid levels[12, 54]. In our analysis of the gross appearance and organization of *stac3*$^{-/-}$ larvae muscle fibers, *stac3* was found to play a pivotal role in establishing F-actin and slow muscle fiber functional coordination to generate strength and execute active contractions. Despite *Stac3* nutrient-sensing activity, its potential functional role via lipid metabolism has barely been studied in animal models for NAM. Our studies found that deletion of 10 base pairs in *stac3* had no impact on neutral lipid levels in 4 dpf *stac3*$^{-/-}$ fish. Yet, higher levels of neutral lipids were measured in *stac3*$^{-/-}$ compared to *stac3*$^{+/+}$ and *stac3*$^{+/-}$ control larvae on 5 dpf and maintained through 7 dpf. Taken together, these findings suggest that *stac3* acts as an age-specific metabolic regulator in the transformation from unhatched to hatched zebrafish larvae, by controlling lipid (energy) utilization in early life. Five dpf is an ideal age for

investigating skeletal muscle formation while the effect of metabolic changes on muscle fibers organization can be examined at 7 pf in zebrafish. We observed that the damaged organization of F-actin and slow muscle fibers could play a role in the progression of myopathy. Due to a significant role in energy processing, utilization, and generating strength in humans, we suggest that improvement of slow muscle fiber integrity could delay the progression of muscle diseases (congenital myopathies)[55].

According to the literature[56, 57], the yolk is considered a reservoir of metabolically active nutrients needed for the embryonic growth and development of an organism. Around 3 dpf, yolk sac contains vascular network with compartments delimited by veins, while reduction of yolk sac is seen as embryo utilizes it at 4 dpf[37, 58]. Inherently, zebrafish larvae utilize maternally acquired lipids as an energy source for the routine biological functions until the age of ~5 dpf, while the larva transforms into adult zebrafish with rapid development of musculoskeletal system[36, 59]. The yolk syncytial layer (YSL) is important for the delivery of lipids during the larval growth and development[58]. With functional activity in early-life stages and nutrients' demand in an organism, lipids are essential for formation of organ and tissue types e.g. heart, liver, intestine, pancreas, and other vascularized regions, including skeletal muscle. Recently, it was reported that intramuscular adipose tissue is increased in dystrophy and neuromuscular disease patients compared with control individuals[60]; it now is evident that NAM's etiology is similar. Altogether, the persistence of altered metabolic condition, which can deteriorate muscle function in NAM, is under-appreciated. We found that *stac3* KO larvae retained neutral lipids, mostly at the yolk sac region, even at the age when the exogenous feeding becomes necessary (7 dpf). At this age, neutral lipids were less visible in *stac3*$^{+/+}$ and *stac3*$^{+/-}$ control groups. Consequently, we speculate that the intact *stac3* enables nutrient sensing for growth of the musculoskeletal system, resulting in rapid muscle contractions, and larvae survival. Loss of *stac3* manifests by accumulation of neutral lipids, which is detrimental in the early growth stages of zebrafish larvae[61]. Storage of

neutral lipids might contribute to a systemic metabolic dysfunction by lipotoxicity/senescence effect on cytoskeleton organization of the larvae. Of interest, the family of STAC proteins has been associated with nuclear factor-*k*B and C/EBP in controlling senescence in the course of muscle cell proliferation and differentiation[16]. We found that senescence-associated beta-gal staining was accentuated in the yolk sac region of *stac3*$^{-/-}$ at 6 dpf. Taken together, at early or late-embryonic stages, skeletal muscle cells might encounter lipotoxicity-induced stress, which triggers their dormant state through cellular senescence[31]. Prolonged accumulation of lipids via lipotoxicity in *stac3* knockout zebrafish could further contribute to unfavorable conditions (signals) that cause tissue (i.e. muscle) deterioration and larval death. Comprehensive studies will be required to understand lipid metabolism-driven vertebrate developmental transformations in early ZF life.

Physiologically, STAC3 oversees the biochemical relationship between calcium sensing (DHPR) and calcium-releasing (RYR1) receptors at the sarcoplasmic reticulum in skeletal muscle[20, 43], with calcium homeostasis being essential for active contractions, tissue formation, maturation, and regeneration[62]. In the present work, *stac3*$^{-/-}$ larvae were found to have lower concentrations of calcium and upregulation of *ryr1a* in an early patterning of skeletal muscle fibers. These findings compelled us to draw a working hypothesis that escalated lipid levels can directly reduce muscle contractions, as manifested by (a) a delay of embryo hatching due to muscle weakness, (b) impaired Ca^{2+} release via *ryr1a*, and (c) damaged organization of F-actin and slow muscle fibers (Fig9). In sum, these *stac3* KO phenotypes suggest paralyzed muscle function manifested as a significantly reduced locomotion on 5 dpf. Recent case studies from Turkey[63], France[64] and Russia[65] suggested that pathophysiology of myopathy progression is comparable to NAM disease phenotypic outcome in humans. 36% of individuals afflicted with Native American myopathy (NAM) died by the age of 18 years[12]. We hypothesized that caffeine could be an effective therapeutic molecule to a betterment of congenital myopathies due to its key mechanistic

biochemical actions across muscle and other tissues[20, 41, 42]. Indeed, our findings suggest that there is increased trend in the survival of the 5mM caffeine treatment in deformed *stac3* larvae at 5 dpf, while 5mM caffeine treatment revealed rather an opposite effect on *stac3*$^{-/-}$ at 7 dpf. Hypothetically, the biochemical action of caffeine could be inhibited at the age of external feeding should start, which is ~7 dpf. Thus, we postulate that our *stac3* knockout zebrafish, established for NAM is a lipid-related human congenital myopathy (lipid storage myopathy). Altogether, exploring early life's genetic mechanisms using *stac3*$^{-/-}$ zebrafish model are frontiers for repressing muscle fiber degeneration and refining muscle function maintaining lipid homeostasis in NAM disease during the course of muscle fibers formation.

Animal models are the gold standard for gaining pre-clinical insights into various diseases, due to their anatomical and morphological resemblance to humans[66]. Of late, modeling of human myopathies is achieved by knocking out disease-causing genes by CRISPR/Cas9 technology[67]. The current work demonstrated that *stac3*$^{-/-}$ fish may serve as a potential model for identifying lipid-based biomarkers or small molecules for the early diagnosis or treatment of NAM. Intramuscular adipose tissue is increased in dystrophy and neuromuscular disease patients compared with control individuals. We suggest that *STAC3* has beneficial effects on muscle metabolism by preventing the damage triggered by genetic or metabolic dysfunctions due to abnormally accumulated lipids.

Acknowledgements

We are grateful to Dr. Chen Shochat for her helpful advice in CRISPR. The authors would like to thank Dr. Sergio Szvalb's lab at the Department of the Pathology, Ziv Hospital, Safed, Israel, for the muscle histology. We extend our gratitude to Dr. Daya's lab for allowing us to perform the birefringence assay at the Faculty of Marine Sciences, Ruppin Academic Center, Mikhmoret, Israel.

Conflict of interest

The authors declare no conflict of interest.

Data availability

Data generated or utilized in this study can be found in online data repository source.

Funding

Supported by grant ISF-1121/19 from Israel Science Foundation and ISF-2058/21 from China-Israel Cooperation.

Supplementary materials

The supplementary materials and figures related to this article can be accessed through online version of the manuscript.

Author Contributions

RD: Conceptualization, investigation, data curation, data analysis, writing original draft, manuscript review and editing, DK: Conceptualization, data curation, funding acquisition, project administration, supervision, manuscript review and editing. HFZ: investigation, data curation, data analysis and manuscript review and editing. All the authors contributed to the article and approved the version submitted for the publication.

References

1. McLeod, M., Breen, L., Hamilton, D.L., and Philp, A. Live strong and prosper: the importance of skeletal muscle strength for healthy ageing.
2. Gineste, C., and Laporte, J. (2023). Therapeutic approaches in different congenital myopathies. Current Opinion in Pharmacology 68, 102328.
3. Huang, K., Bi, F., and Huan, Y. (2021). A systematic review and meta-analysis of the prevalence of congenital myopathy. Frontiers in neurology, 1959.
4. Gineste, C., and Laporte, J. Therapeutic approaches in different congenital myopathies.

562 5. Tolchin, D., Yeager, J.P., Prasad, P., Dorrani, N., Russi, A.S., Martinez-Agosto, J.A., Haseeb,
563 A., Angelozzi, M., Santen, G.W.E., Ruivenkamp, C., et al. De Novo SOX6 Variants Cause
564 a Neurodevelopmental Syndrome Associated with ADHD, Craniosynostosis, and
565 Osteochondromas.
566 6. Claeys, K.G. (2020). Congenital myopathies: an update. Developmental Medicine & Child
567 Neurology 62, 297-302.
568 7. Ogasawara, M., and Nishino, I. (2023). A review of major causative genes in congenital
569 myopathies. Journal of Human Genetics 68, 215-225.
570 8. Mendieta-Serrano, M.A., Dhar, S., Ng, B.H., Narayanan, R., Lee, J.J.Y., Ong, H.T., Toh, P.J.Y.,
571 Röllin, A., Roy, S., and Saunders, T.E. (2022). Slow muscles guide fast myocyte fusion to
572 ensure robust myotome formation despite the high spatiotemporal stochasticity of fusion
573 events. Developmental Cell 57, 2095-2110.e2095.
574 9. Zempo, B., Yamamoto, Y., Williams, T., and Ono, F. Synaptic silencing of fast muscle is
575 compensated by rewired innervation of slow muscle. Science Advances 6, eaax8382.
576 10. Jackson, H.E., Ono, Y., Wang, X., Elworthy, S., Cunliffe, V.T., and Ingham, P.W. (2015). The
577 role of Sox6 in zebrafish muscle fiber type specification. Skeletal Muscle 5, 2.
578 11. Li, S., Wen, H., and Du, S. Defective sarcomere organization and reduced larval locomotion
579 and fish survival in slow muscle heavy chain 1 (smyhc1) mutants.
580 12. Stamm, D.S., Aylsworth, A.S., Stajich, J.M., Kahler, S.G., Thorne, L.B., Speer, M.C., and
581 Powell, C.M. (2008). Native American myopathy: Congenital myopathy with cleft palate,
582 skeletal anomalies, and susceptibility to malignant hyperthermia. American Journal of
583 Medical Genetics Part A 146A, 1832-1841.
584 13. Miller, D.M., Daly, C., Aboelsaod, E.M., Gardner, L., Hobson, S.J., Riasat, K., Shepherd, S.,
585 Robinson, R.L., Bilmen, J.G., Gupta, P.K., et al. Genetic epidemiology of malignant
586 hyperthermia in the UK.

14. Rufenach, B., and Van Petegem, F. Structure and function of STAC proteins: Calcium channel modulators and critical components of muscle excitation-contraction coupling.

15. Cong, X., Doering, J., Mazala, D.A., Chin, E.R., Grange, R.W., and Jiang, H. (2016). The SH3 and cysteine-rich domain 3 (Stac3) gene is important to growth, fiber composition, and calcium release from the sarcoplasmic reticulum in postnatal skeletal muscle. Skeletal muscle 6, 1-17.

16. Bower, N.I., de la Serrana Dg Fau - Cole, N.J., Cole Nj Fau - Hollway, G.E., Hollway Ge Fau - Lee, H.-T., Lee Ht Fau - Assinder, S., Assinder S Fau - Johnston, I.A., and Johnston, I.A. Stac3 is required for myotube formation and myogenic differentiation in vertebrate skeletal muscle.

17. Saini-Chohan, H.K., Mitchell Rw Fau - Vaz, F.M., Vaz Fm Fau - Zelinski, T., Zelinski T Fau - Hatch, G.M., and Hatch, G.M. Delineating the role of alterations in lipid metabolism to the pathogenesis of inherited skeletal and cardiac muscle disorders: Thematic Review Series: Genetics of Human Lipid Diseases.

18. Seyssel, K., Alligier, M., Meugnier, E., Chanseaume, E., Loizon, E., Canto, C., Disse, E., Lambert-Porcheron, S., Brozek, J., Blond, E., et al. (2014). Regulation of Energy Metabolism and Mitochondrial Function in Skeletal Muscle During Lipid Overfeeding in Healthy Men. The Journal of Clinical Endocrinology & Metabolism 99, E1254-E1262.

19. Shimano, H., and Sato, R. (2017). SREBP-regulated lipid metabolism: convergent physiology — divergent pathophysiology. Nature Reviews Endocrinology 13, 710-730.

20. Linsley, J.W., Hsu, I.-U., Groom, L., Yarotskyy, V., Lavorato, M., Horstick, E.J., Linsley, D., Wang, W., Franzini-Armstrong, C., and Dirksen, R.T. (2017). Congenital myopathy results from misregulation of a muscle Ca2+ channel by mutant Stac3. Proceedings of the National Academy of Sciences 114, E228-E236.

611 21. Rufenach, B., Christy, D., Flucher, B.E., Bui, J.M., Gsponer, J., Campiglio, M., and Van
612 Petegem, F. Multiple Sequence Variants in STAC3 Affect Interactions with Ca(V)1.1 and
613 Excitation-Contraction Coupling.
614 22. Horstick, E.J., Linsley, J.W., Dowling, J.J., Hauser, M.A., McDonald, K.K., Ashley-Koch, A.,
615 Saint-Amant, L., Satish, A., Cui, W.W., and Zhou, W. (2013). Stac3 is a component of the
616 excitation–contraction coupling machinery and mutated in Native American myopathy.
617 Nature communications 4, 1952.
618 23. Berger, J., and Currie, P.D. Zebrafish models flex their muscles to shed light on muscular
619 dystrophies.
620 24. Sztal, T.E., Zhao, M., Williams, C., Oorschot, V., Parslow, A.C., Giousoh, A., Yuen, M., Hall,
621 T.E., Costin, A., Ramm, G., et al. (2015). Zebrafish models for nemaline myopathy reveal
622 a spectrum of nemaline bodies contributing to reduced muscle function. Acta
623 Neuropathologica 130, 389-406.
624 25. Daya, A., Donaka, R., and Karasik, D. (2020). Zebrafish models of sarcopenia. Disease
625 Models & Mechanisms 13, dmm042689.
626 26. Mesika, A., Nadav, G., Shochat, C., Kalfon, L., Jackson, K., Khalaileh, A., Karasik, D., and
627 Falik-Zaccai, T.C. (2022). NGLY1 Deficiency Zebrafish Model Manifests Abnormalities of
628 the Nervous and Musculoskeletal Systems. Frontiers in Cell and Developmental Biology
629 10.
630 27. Li, H., Xu, J., Bian, Y.-H., Rotllant, P., Shen, T., Chu, W., Zhang, J., Schneider, M., and Du,
631 S.J. (2011). Smyd1b_tv1, a Key Regulator of Sarcomere Assembly, Is Localized on the M-
632 Line of Skeletal Muscle Fibers. PLOS ONE 6, e28524.
633 28. Kishi, S., Bayliss, P.E., Uchiyama, J., Koshimizu, E., Qi, J., Nanjappa, P., Imamura, S., Islam,
634 A., Neuberg, D., Amsterdam, A., et al. (2008). The Identification of Zebrafish Mutants
635 Showing Alterations in Senescence-Associated Biomarkers. PLOS Genetics 4, e1000152.

636 29. Livne, H., Avital, T., Ruppo, S., Harazi, A., Mitrani-Rosenbaum, S., and Daya, A. (2022).
637 Generation and characterization of a novel gne Knockout Model in Zebrafish. Frontiers in
638 Cell and Developmental Biology 10.
639 30. Sokoloff, A.J., Yang, B., Li, H., and Burkholder, T.J. (2007). Immunohistochemical
640 characterization of slow and fast myosin heavy chain composition of muscle fibres in the
641 styloglossus muscle of the human and macaque (Macaca rhesus). Arch Oral Biol 52, 533-
642 543.
643 31. Stewart, M.A., Franks-Skiba, K., Chen, S., and Cooke, R. (2010). Myosin ATP turnover rate
644 is a mechanism involved in thermogenesis in resting skeletal muscle fibers. Proc Natl Acad
645 Sci U S A 107, 430-435.
646 32. Yamamoto, M., Legendre, N.P., Biswas, A.A., Lawton, A., Yamamoto, S., Tajbakhsh, S.,
647 Kardon, G., and Goldhamer, D.J. Loss of MyoD and Myf5 in Skeletal Muscle Stem Cells
648 Results in Altered Myogenic Programming and Failed Regeneration.
649 33. Cao, Y., Kumar Rm Fau - Penn, B.H., Penn Bh Fau - Berkes, C.A., Berkes Ca Fau -
650 Kooperberg, C., Kooperberg C Fau - Boyer, L.A., Boyer La Fau - Young, R.A., Young Ra
651 Fau - Tapscott, S.J., and Tapscott, S.J. Global and gene-specific analyses show distinct
652 roles for Myod and Myog at a common set of promoters.
653 34. Reinholt, B.M., Ge, X., Cong, X., Gerrard, D.E., and Jiang, H. (2013). Stac3 is a novel
654 regulator of skeletal muscle development in mice. PloS one 8, e62760.
655 35. Shi, H., Verma, M., Zhang, L., Dong, C., Flavell, R.A., and Bennett, A.M. (2013). Improved
656 regenerative myogenesis and muscular dystrophy in mice lacking Mkp5. The Journal of
657 Clinical Investigation 123, 2064-2077.
658 36. Quinlivan, V.H., and Farber, S.A. (2017). Lipid Uptake, Metabolism, and Transport in the
659 Larval Zebrafish. Frontiers in Endocrinology 8.

660 37. Jiang, K., Pichol-Thievend, C., Neufeld, Z., and Francois, M. Assessment of heterogeneity in
661 collective endothelial cell behavior with multicolor clonal cell tracking to predict
662 arteriovenous remodeling.
663 38. Stamm, D.S., Aylsworth As Fau - Stajich, J.M., Stajich Jm Fau - Kahler, S.G., Kahler Sg Fau
664 - Thorne, L.B., Thorne Lb Fau - Speer, M.C., Speer Mc Fau - Powell, C.M., and Powell,
665 C.M. Native American myopathy: congenital myopathy with cleft palate, skeletal
666 anomalies, and susceptibility to malignant hyperthermia.
667 39. Kepser, L.-J., Damar, F., De Cicco, T., Chaponnier, C., Prószyński, T.J., Pagenstecher, A.,
668 and Rust, M.B. (2019). CAP2 deficiency delays myofibril actin cytoskeleton differentiation
669 and disturbs skeletal muscle architecture and function. Proceedings of the National
670 Academy of Sciences 116, 8397-8402.
671 40. Barcelos, R.P., Lima, F.D., Carvalho, N.R., Bresciani, G., and Royes, L.F. Caffeine effects on
672 systemic metabolism, oxidative-inflammatory pathways, and exercise performance.
673 41. Tallis, J., James Rs Fau - Cox, V.M., Cox Vm Fau - Duncan, M.J., and Duncan, M.J. The
674 effect of physiological concentrations of caffeine on the power output of maximally and
675 submaximally stimulated mouse EDL (fast) and soleus (slow) muscle.
676 42. Gonçalves, D.F., Tassi, C.C., Amaral, G.P., Stefanello, S.T., Dalla Corte, C.L., Soares, F.A.,
677 Posser, T., Franco, J.L., and Carvalho, N.R. Effects of caffeine on brain antioxidant status
678 and mitochondrial respiration in acetaminophen-intoxicated mice.
679 43. Nelson, B.R., Wu, F., Liu, Y., Anderson, D.M., McAnally, J., Lin, W., Cannon, S.C., Bassel-
680 Duby, R., and Olson, E.N. (2013). Skeletal muscle-specific T-tubule protein STAC3
681 mediates voltage-induced Ca2+ release and contractility. Proceedings of the National
682 Academy of Sciences 110, 11881-11886.

683 44. Conerly, M.L., Yao, Z., Zhong, J.W., Groudine, M., and Tapscott, S.J. Distinct Activities of
684 Myf5 and MyoD Indicate Separate Roles in Skeletal Muscle Lineage Specification and
685 Differentiation.
686 45. Ganassi, M., Badodi, S., Wanders, K., Zammit, P.S., and Hughes, S.M. (2020). Myogenin is
687 an essential regulator of adult myofibre growth and muscle stem cell homeostasis. eLife 9,
688 e60445.
689 46. Mok, G.F., Mohammed, R.H., and Sweetman, D. Expression of myogenic regulatory factors
690 in chicken embryos during somite and limb development.
691 47. Malila, Y., Thanatsang, K.V., Sanpinit, P., Arayamethakorn, S., Soglia, F., Zappaterra, M.,
692 Bordini, M., Sirri, F., Rungrassamee, W., Davoli, R., et al. (2022). Differential expression
693 patterns of genes associated with metabolisms, muscle growth and repair in Pectoralis
694 major muscles of fast- and medium-growing chickens. PLOS ONE 17, e0275160.
695 48. Wen, C., Jiang, X., Ding, L., Wang, T., and Zhou, Y. (2017). Effects of dietary methionine on
696 breast muscle growth, myogenic gene expression and IGF-I signaling in fast- and slow-
697 growing broilers. Scientific Reports 7, 1924.
698 49. Coppens, S., Barnard, A.M., Puusepp, S., Pajusalu, S., Õunap, K., Vargas-Franco, D., Bruels,
699 C.C., Donkervoort, S., Pais, L., Chao, K.R., et al. (2021). A form of muscular dystrophy
700 associated with pathogenic variants in JAG2. The American Journal of Human Genetics
701 108, 840-856.
702 50. Jungbluth, H., Ochala, J., Treves, S., and Gautel, M. (2017). Current and future therapeutic
703 approaches to the congenital myopathies. Seminars in Cell & Developmental Biology 64,
704 191-200.
705 51. Schessl, J., Taratuto, A.L., Sewry, C., Battini, R., Chin, S.S., Maiti, B., Dubrovsky, A.L., Erro,
706 M.G., Espada, G., Robertella, M., et al. (2009). Clinical, histological and genetic

characterization of reducing body myopathy caused by mutations in FHL1. Brain 132, 452-464.

52. Böhm, J., Vasli, N., Malfatti, E., Le Gras, S., Feger, C., Jost, B., Monnier, N., Brocard, J., Karasoy, H., Gérard, M., et al. (2013). An Integrated Diagnosis Strategy for Congenital Myopathies. PLOS ONE 8, e67527.

53. Cassandrini, D., Trovato, R., Rubegni, A., Lenzi, S., Fiorillo, C., Baldacci, J., Minetti, C., Astrea, G., Bruno, C., Santorelli, F.M., et al. (2017). Congenital myopathies: clinical phenotypes and new diagnostic tools. Italian Journal of Pediatrics 43, 101.

54. Stamm, D., Powell, C., Stajich, J., Zismann, V., Stephan, D., Chesnut, B., Aylsworth, A., Kahler, S., Deak, K., and Gilbert, J. (2008). Novel congenital myopathy locus identified in Native American Indians at 12q13. 13-14.1. Neurology 71, 1764-1769.

55. Talbot, J., and Maves, L. Skeletal muscle fiber type: using insights from muscle developmental biology to dissect targets for susceptibility and resistance to muscle disease.

56. Miyares, R.L., de Rezende, V.B., and Farber, S.A. Zebrafish yolk lipid processing: a tractable tool for the study of vertebrate lipid transport and metabolism.

57. Fraher, D., Sanigorski, A., Mellett, Natalie A., Meikle, Peter J., Sinclair, Andrew J., and Gibert, Y. (2016). Zebrafish Embryonic Lipidomic Analysis Reveals that the Yolk Cell Is Metabolically Active in Processing Lipid. Cell Reports 14, 1317-1329.

58. Goi, M., and Childs, S.J. (2016). Patterning mechanisms of the sub-intestinal venous plexus in zebrafish. Developmental Biology 409, 114-128.

59. Edinburgh, R.M., Bradley, H.E., Abdullah, N.-F., Robinson, S.L., Chrzanowski-Smith, O.J., Walhin, J.-P., Joanisse, S., Manolopoulos, K.N., Philp, A., Hengist, A., et al. (2020). Lipid Metabolism Links Nutrient-Exercise Timing to Insulin Sensitivity in Men Classified as Overweight or Obese. The Journal of Clinical Endocrinology & Metabolism 105, 660-676.

731 60. Goodpaster, B.H., Bergman, B.C., Brennan, A.M., and Sparks, L.M. (2022). Intermuscular
732 adipose tissue in metabolic disease. Nature Reviews Endocrinology.
733 61. Yoganantharjah, P., Byreddy Ar Fau - Fraher, D., Fraher D Fau - Puri, M., Puri M Fau - Gibert,
734 Y., and Gibert, Y. Rapid quantification of neutral lipids and triglycerides during zebrafish
735 embryogenesis.
736 62. Sinha, S., Elbaz-Alon, Y., and Avinoam, O. (2022). Ca2+ as a coordinator of skeletal muscle
737 differentiation, fusion and contraction. The FEBS Journal 289, 6531-6542.
738 63. Telegrafi, A, Webb, B, Robbins, S.M., Speck-Martins, C.E., FitzPatrick, D., Fleming, L.A,
739 Redett, R., Dufke, A., Houge, G, van Harssel, J.J.T., et al. Identification of STAC3 variants
740 in non-Native American families with overlapping features of Carey-Fineman-Ziter
741 syndrome and Moebius syndrome.
742 64. Gromand, M., Gueguen, P., Pervillé, A., Ferroul, F., Morel, G., Harouna, A., Doray, B.,
743 Urtizberea, J.A., Alessandri, J.-L., and Robin, S. (2022). STAC3 related congenital
744 myopathy: A case series of seven Comorian patients. European Journal of Medical
745 Genetics 65, 104598.
746 65. Murtazina, A., Demina, N., Chausova, P., Shchagina, O., Borovikov, A., and Dadali, E. (2022).
747 The First Russian Patient with Native American Myopathy. In Genes.
748 66. Patton, E.E., Zon, L.I., and Langenau, D.M. (2021). Zebrafish disease models in drug
749 discovery: from preclinical modelling to clinical trials. Nature Reviews Drug Discovery 20,
750 611-628.
751 67. Espinosa, K.G., Geissah, S., Groom, L., Volpatti, J., Scott, I, Dirksen, R.T., Zhao, M, and
752 Dowling, J. Characterization of a novel zebrafish model of SPEG-related centronuclear
753 myopathy. LID - 10.1242/dmm.049437.

754

Figure legends

1. Deletion of 10 base pairs (bp) of *stac3* gene in zebrafish

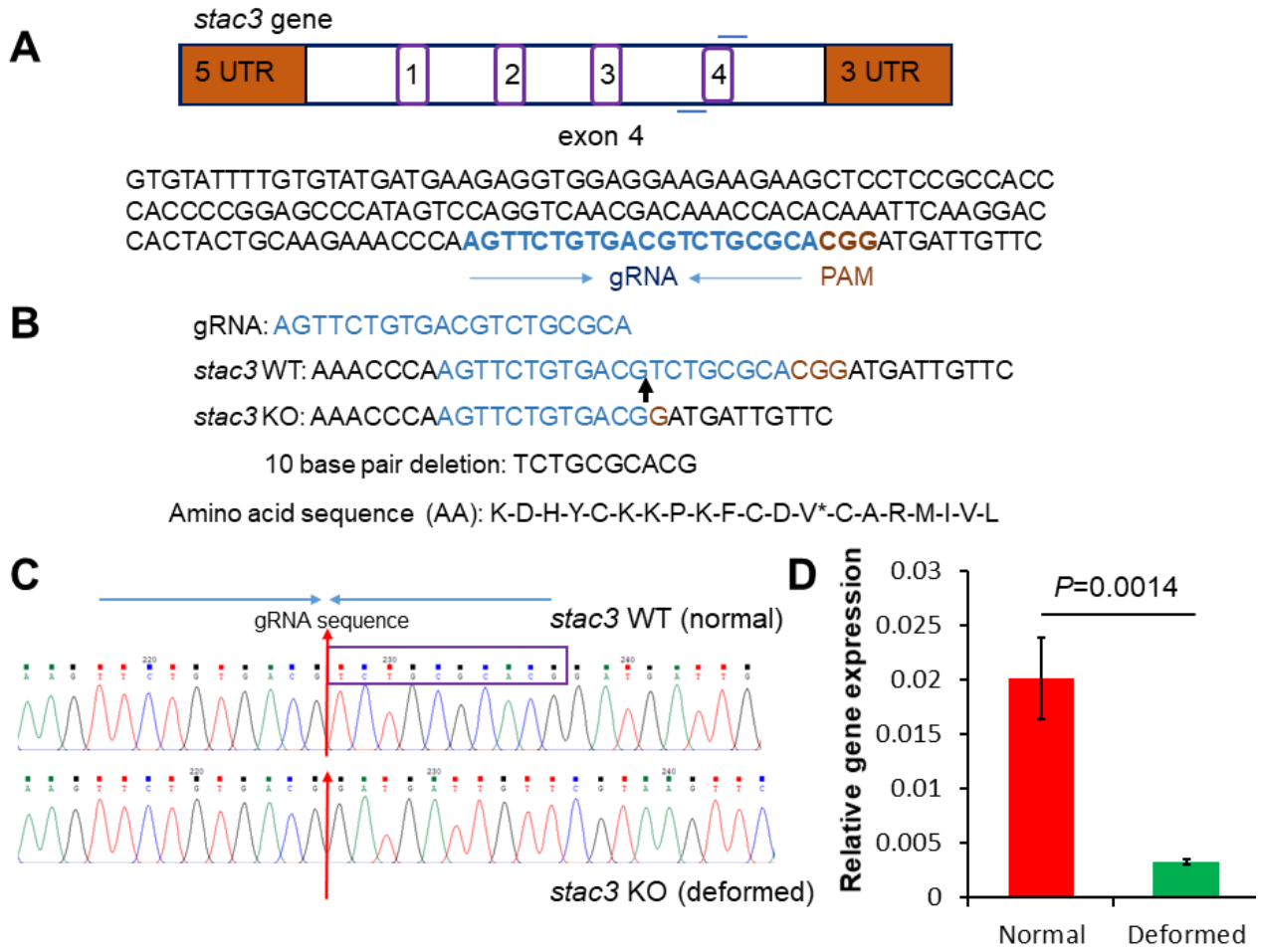

(A, B). Schematic presentation of the *stac3* gene and nucleotide sequence of exon 4 region, which is marked for both guide RNA and PAM sequences, amino acids predicted using Ensembl.org. The stop codon at V78 is shown with asterisk. (C). DNA sequencing of the *stac3* wild type siblings (top), knockout (bottom). The deleted sequence TCTGCGCACG is marked by a violet box, red arrows indicate the starting position of the knockout. (D). RT-PCR analysis showed significant downregulation of *stac3* expression in deformed larvae (knockout) compared to wild type and heterozygous siblings (5 dpf). Data are presented as mean ± standard deviation. T-Test, *p= 0.0014.

2. Delayed hatching of *stac3* $^{-/-}$ (KO) zebrafish larvae

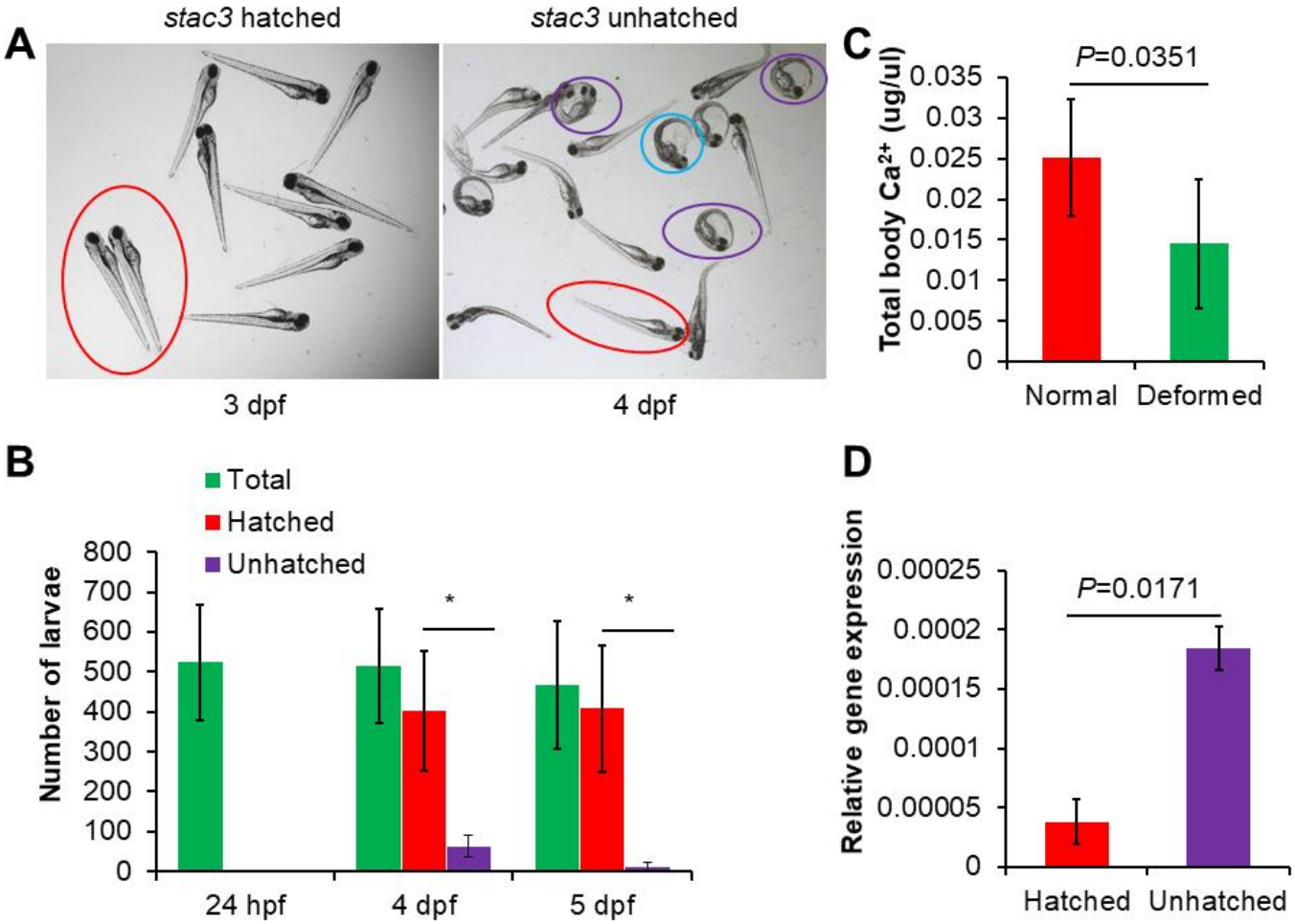

(A). Hatching of *stac3*$^{-/-}$ larvae at 3 and 4 days post-fertilization (dpf). The blue circle marks larvae attempting to come out of the chorion (delayed hatching: knockout), while violet color indicates unhatched (knockout) larvae, hatched (*stac3*$^{+/+}$ and *stac3*$^{+/-}$: wild type and heterozygous siblings) larvae are outlined in red. (B). Percentage of delayed hatching of *stac3*$^{-/-}$ larvae at different time points, T-Test, *p=0.018 (4 dpf), *p=0.012 (5 dpf). (C). Whole-body Ca^{2+} levels in *stac3*$^{-/-}$ larvae, T-Test, *p=0.0351. (D). Ryanodine receptor 1a (*ryr1a*) gene expression, T-Test, *p=0.0171. Data are presented as mean ± standard deviation.

3. Slow muscle myosin staining of KO larvae

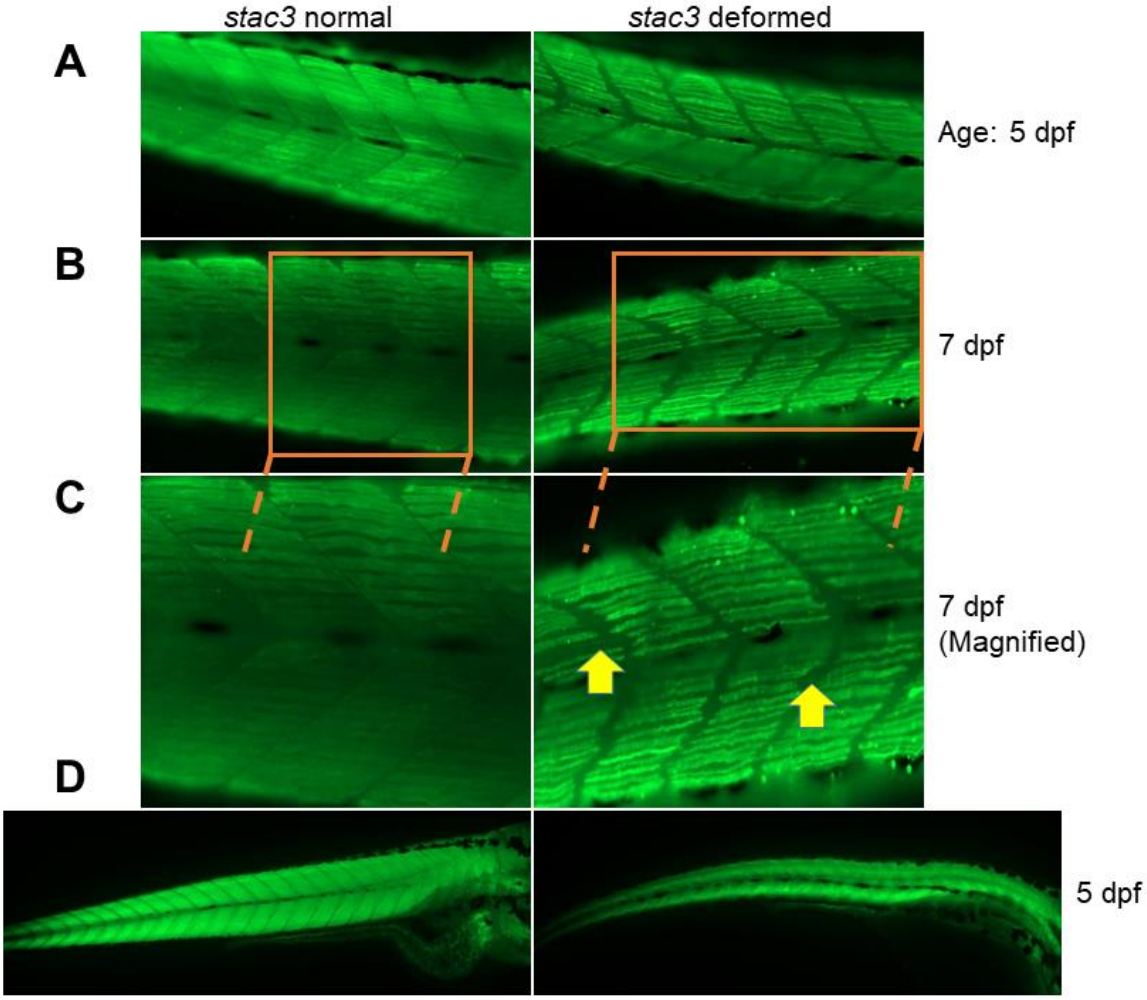

(A). Whole-mount immunostaining of slow muscle myosin isoforms with anti-Myhc1 antibody, in the trunk region, *stac3* KO larvae showed thin, curly muscle fibers, and smaller gaps compared to *stac3* WT and heterozygous fish at 5 dpf. (B). In the trunk region, *stac3* KO larvae (right) exhibited protruding breaks between somite boundaries compared to muscle fibers patterning's in $stac3^{+/+}$ and $stac3^{+/-}$ control siblings (left) at 7 dpf. (C). Bottom panels (B) are magnified; protruding breaks between somite boundaries are marked with yellow arrow heads. (D). Wild type and heterozygous *stac3* and *stac3* knockout larvae stained with phalloidin at 5 dpf. Reduced amounts of filamentous (F-actin) fibers were noted in whole body of *stac3* knockout larvae (right) compared to $stac3^{+/+}$ and $stac3^{+/-}$ control siblings (left).

4. Knockout of *stac3* alters myogenesis in zebrafish larvae

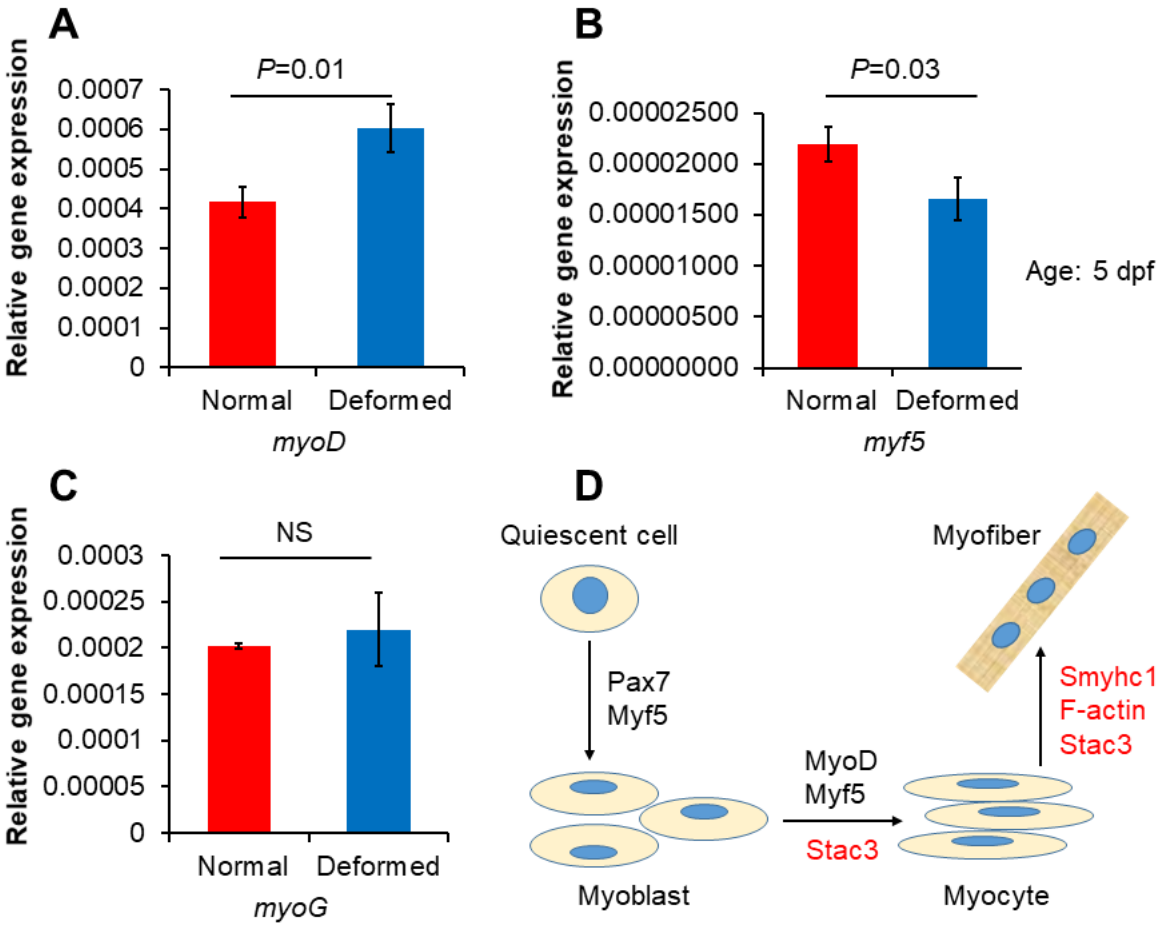

(A). RT-PCR analysis revealed that gene expression of *myoD* was significantly upregulated in *stac3*$^{-/-}$ larvae compared to *stac3* wild type and heterozygotes (B). *myf5* gene expression was significantly downregulated in *stac3*$^{-/-}$ larvae compared to wild type and heterozygous siblings. (C). *stac3* knockout had no effect on mRNA levels of *myoG*. (D). A suggested mechanistic action of *stac3* in early muscle formation (red color denote functional regulators). T-Test, *p=0.01, *p=0.03, Non-significant (NS), n=10 animals for each group. Data are presented as mean ± standard deviation.

5. Lipid staining of *stac3* KO larvae using Oil Red O (ORO)

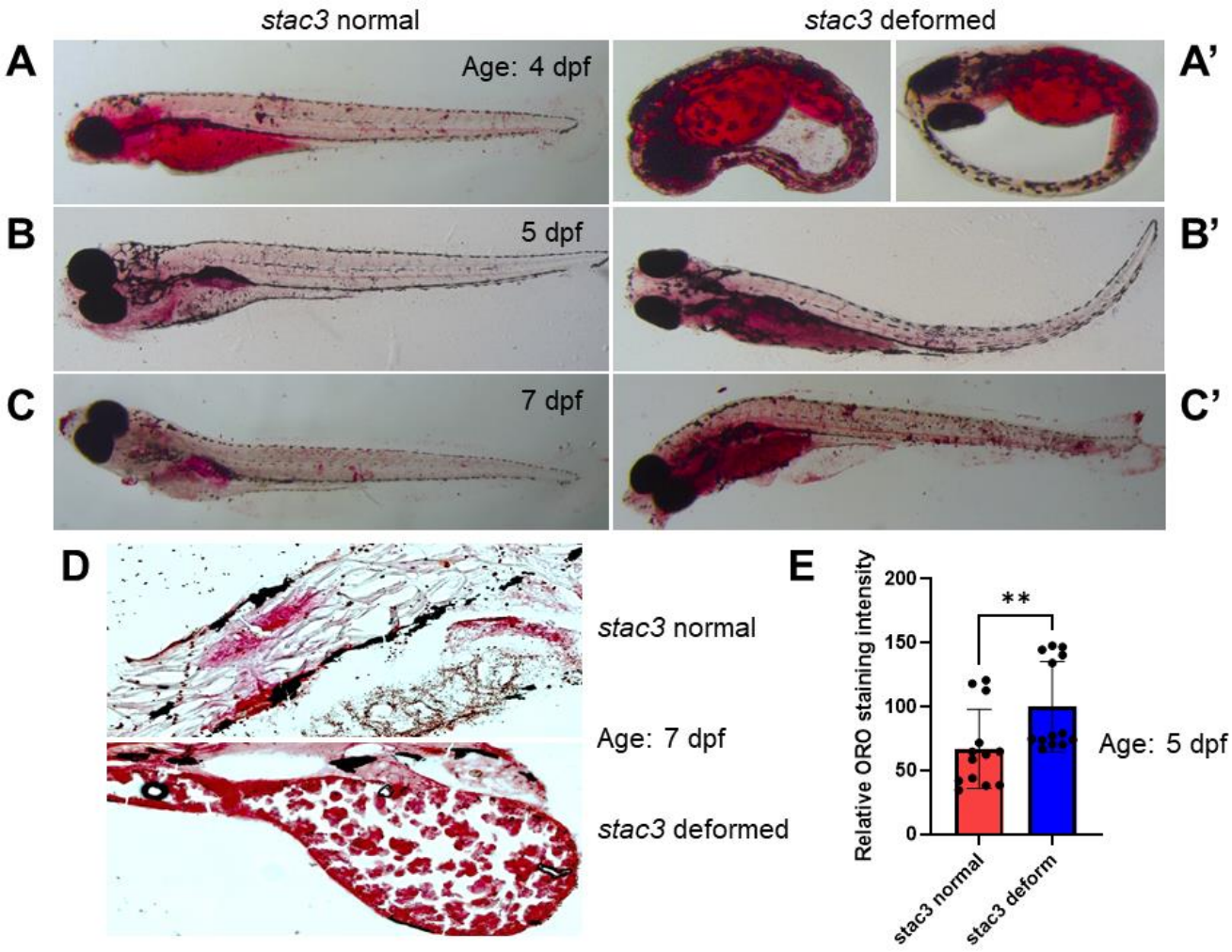

(A-A'). Hatched (*stac3* wild type and heterozygous) and unhatched (*stac3* knockout) larvae were stained with ORO dye for neutral lipid visualization, both groups displayed similar levels of neutral lipids at 4 dpf (scale bar 3 mm). At 5 dpf (B-B') and 7 dpf (C-C': scale bar 3 mm), deformed (*stac3* knockout: B' and C') larvae exhibited higher neutral lipids compared to *stac3* wild type and heterozygous (B and C). (D). OCT based yolk sac sections of *stac3* normal and knockout larvae were stained with ORO dye. *stac3* knockout larvae (bottom) displayed more lipids compared to *stac3* normal (top) at 7 dpf. (E). Quantification red color indicated relative ORO staining intensity of the larvae. At each stage n=15 animals utilized per group. Mann Whitney test, **p=0.0023. Genotype of larvae (n=10) per group was confirmed as described in FigureS1A, B.

6. Death of *stac3* knockout might be due to metabolic dysfunction

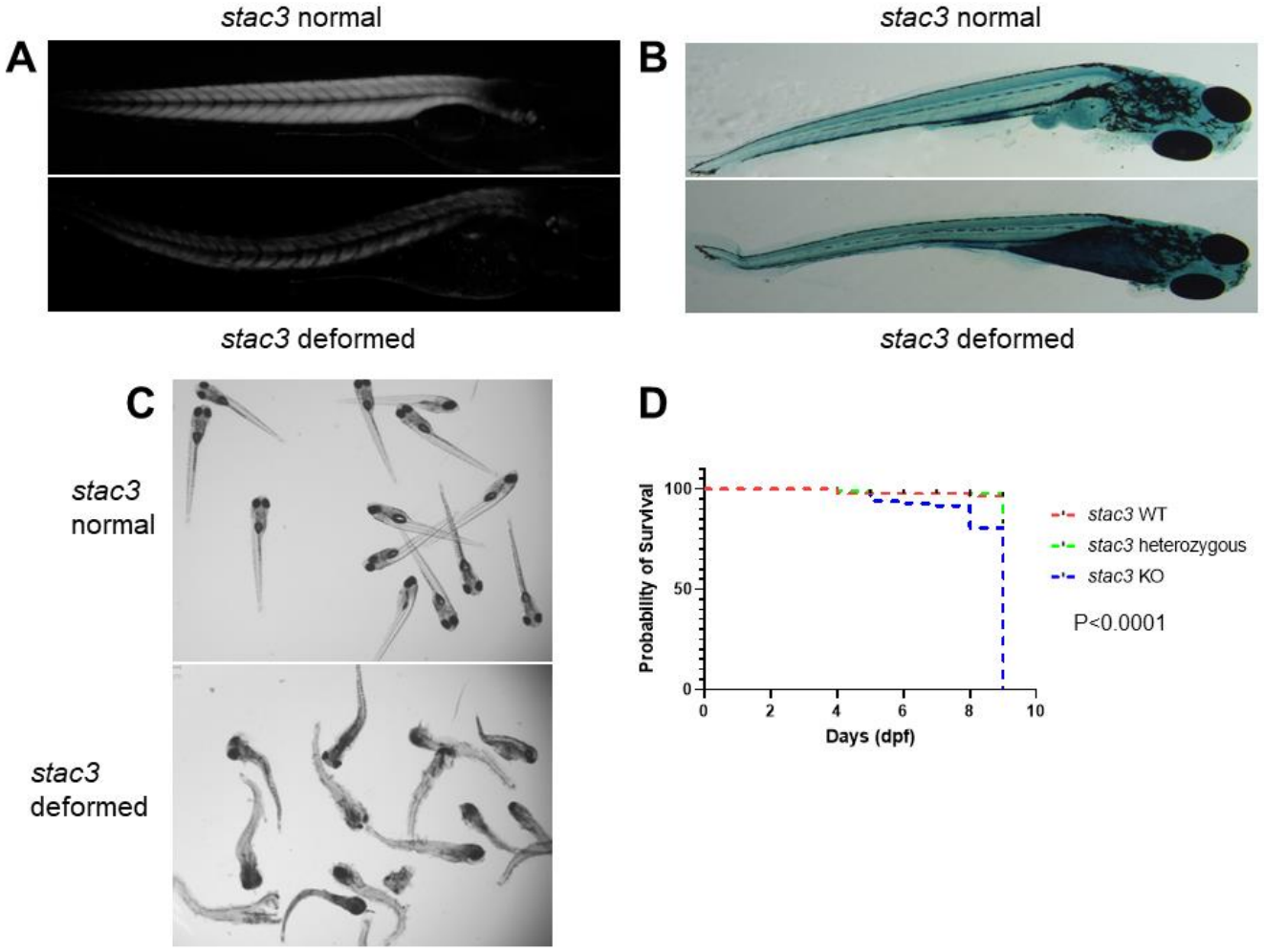

(A). Birefringence assay demonstrated reduced chevron formation of muscle fibers in *stac3* knockout (bottom) compared to wild type *stac3* larvae (top) at 5 dpf. (B). *stac3* knockout larvae exhibited increased cellular senescence mostly in the yolk sac region (bottom) in comparison to wild type *stac3* (top), as demonstrated by SA-β-gal staining at 6 dpf. (C). Dead larvae are identified as *stac3* knockout (bottom) compared to *stac3* wild type and heterozygous siblings (top) at 5 dpf. (D). Survival analysis of *stac3*$^{-/-}$, wild type and heterozygous siblings at 1-10 dpf. Post birefringence analysis, larvae (n=5-10) per group were utilized for genotype confirmation. Log-rank test applied for *stac3* WT, *stac3* heterozygous, and *stac3* KO zebrafish larva groups, ****p<0.0001. The genotype of dead larvae (n=80) was confirmed as described in FigureS1A, B.

7. Swimming performance (locomotion) of *stac3* knockout in early life

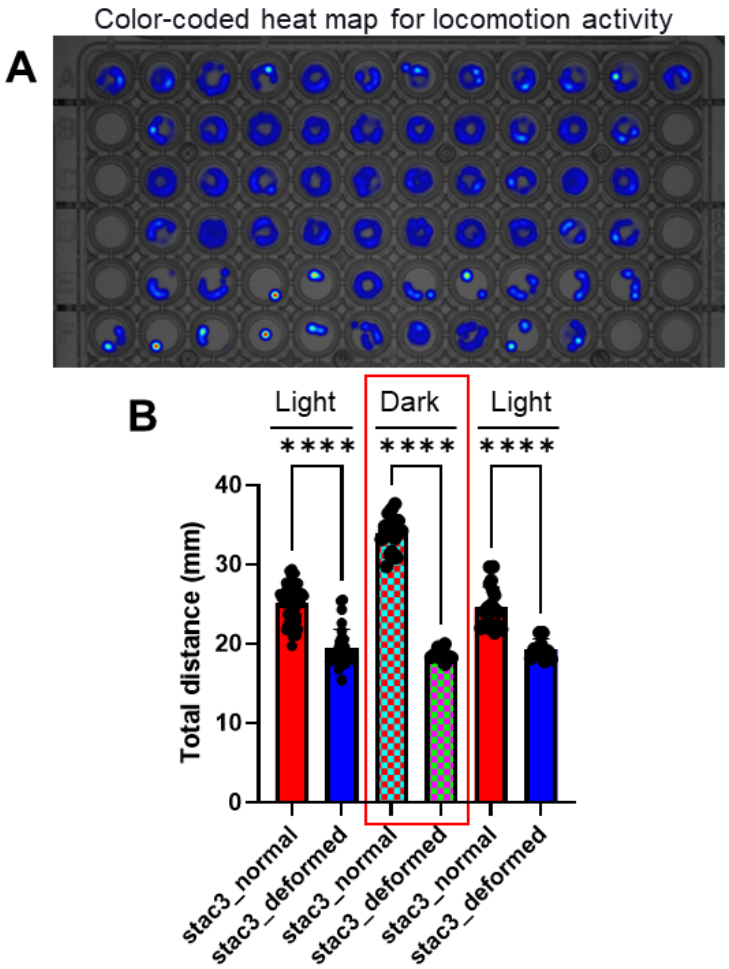

(A). Merged, color-coded heat map for the total distance travelled by each larvae at 5 dpf. The blue color corresponds to a longer distance travelled, while pale yellow-red corresponds to no movement activity. (B). The locomotion tracking protocol included 15 minutes light on, 5 minutes light off, then 5 minutes light on. One-way ANOVA, ****p=0.0001, *stac3*$^{+/+}$ and *stac3*$^{+/-}$ (n=48) and *stac3*$^{-/-}$ (n=22) animals for each group. Genotype of larvae (n=10) per group was confirmed as described in FigureS1A, B. Each dot represents the total distance travelled by the larvae on graph Data are presented as mean ± standard deviation.

8. Survival of the *stac3*$^{-/-}$ larvae at 5 dpf and 7 dpf after caffeine treatment

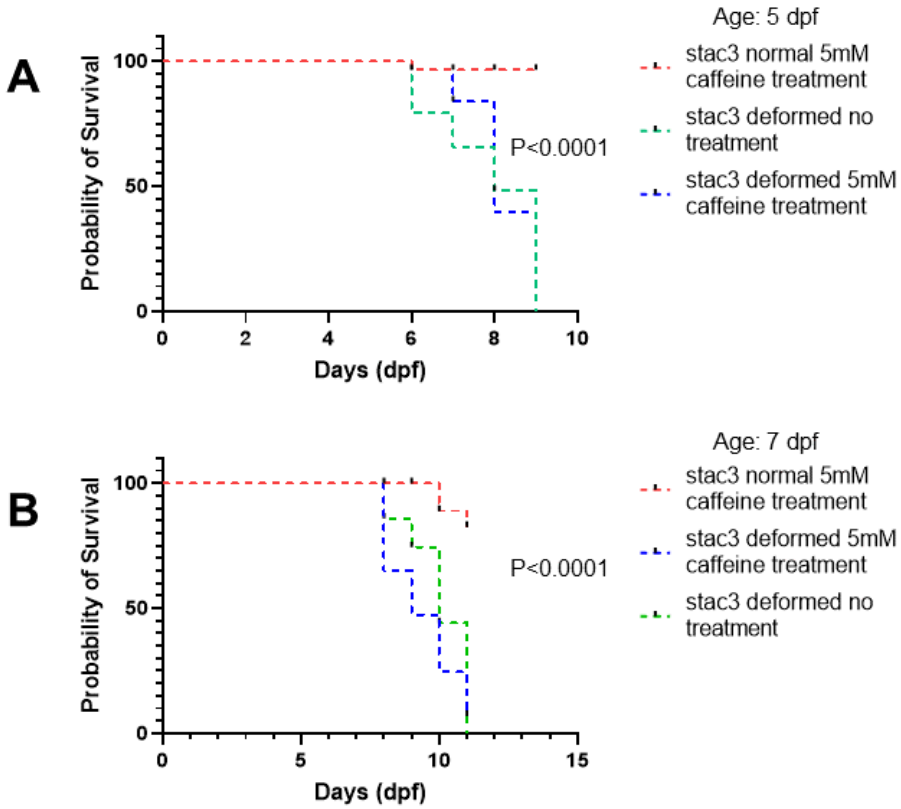

(A-B). Calculation of survival percentage of *stac3* KO (deformed) and *stac3* normal (*stac3*$^{+/+}$ and *stac3*$^{+/-}$ control siblings) zebrafish larvae with and without 5mM caffeine at 5 and 7 dpf. In both age groups, survival analysis was performed in 2-3 replicates, and larvae growth and survival were monitored for 96 hours. Log-rank test applied between treated and untreated deformed *stac3* zebrafish groups, ****p<0.0001.

9. Working model of *stac3* gene in early life of zebrafish

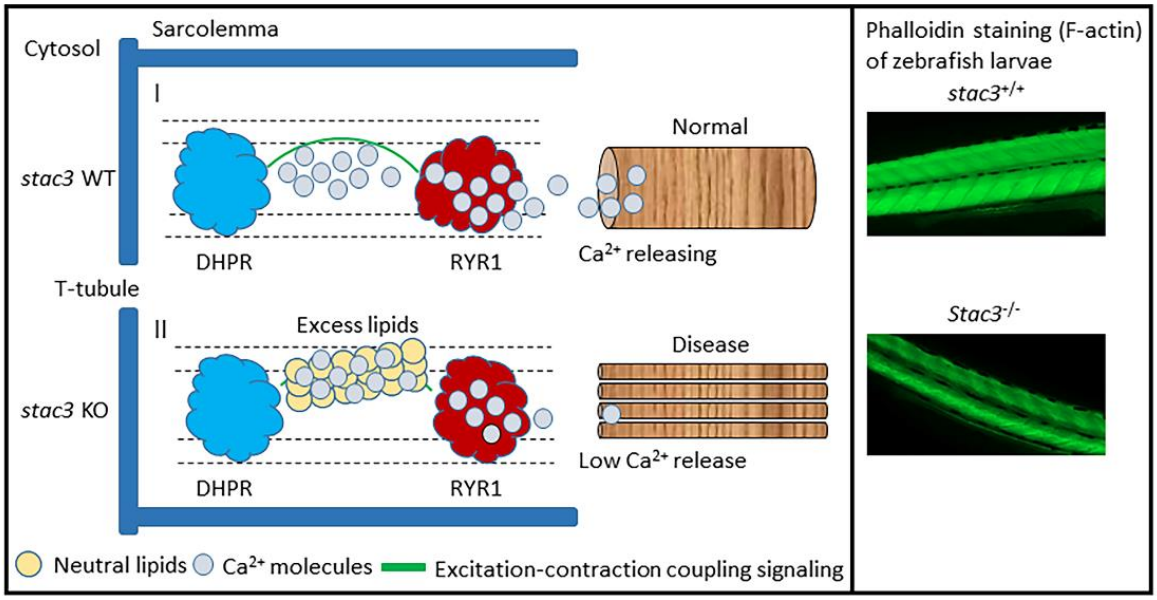

In *stac3* knockout, increased lipids can directly reduce Ca^{2+} release at DHPR via RYR1 (*ryr1a*) receptor which seemingly delays the functional organization of F-actin and slow muscle fibers of zebrafish larva at early life.

Supplementary figures and legends

S1. Knockout confirmation of the *stac3* gene in zebrafish

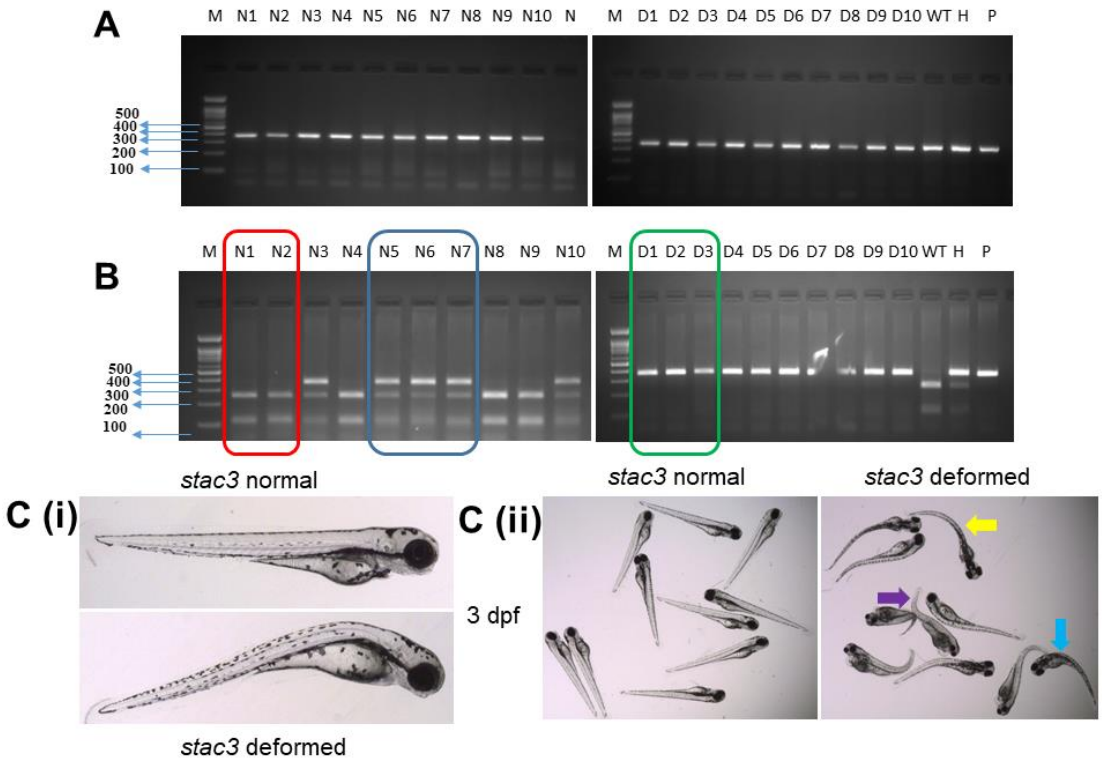

(A). DNA was extracted from wild type and heterozygous and knockout *stac3* larvae at the age of 3 dpf and amplified in a polymerase chain reaction (PCR) using *stac3* gene-specific primers (top). (B). The PCR product was confirmed on a 2% agarose gel, which showed a single band at 363 base pairs (bp). The PCR product was digested using the *FSPI* enzyme. The wild type had two digested DNA products (250 bp and 113 bp, red). The heterozygotes had three digested DNA products (113 bp, 250bp, and 363 bp, blue). The knockout undigested PCR product was a single band at 363 bp (green) (bottom). M-marker, N1-N10 (normal: $stac3^{+/+}$ and $stac3^{+/-}$ siblings): wild type and heterozygous, D1-D10 (deformed: $stac3^{-/-}$): knockout, WT-wild type, H-heterozygote, P-positive control. (C). At 3 days post-fertilization, $stac3^{-/-}$ mutant larvae were distinguishable from

866 *stac3*$^{+/+}$ and *stac3*$^{+/-}$ siblings (i), and displayed multiple congenital musculoskeletal defects, which
867 included bending at the head (blue), trunk (yellow), and tail regions (violet) (ii). Scale bar: 1 mm.

868 **S2. Genotype confirmation of delayed hatching of larvae by sequencing at 4 dpf**

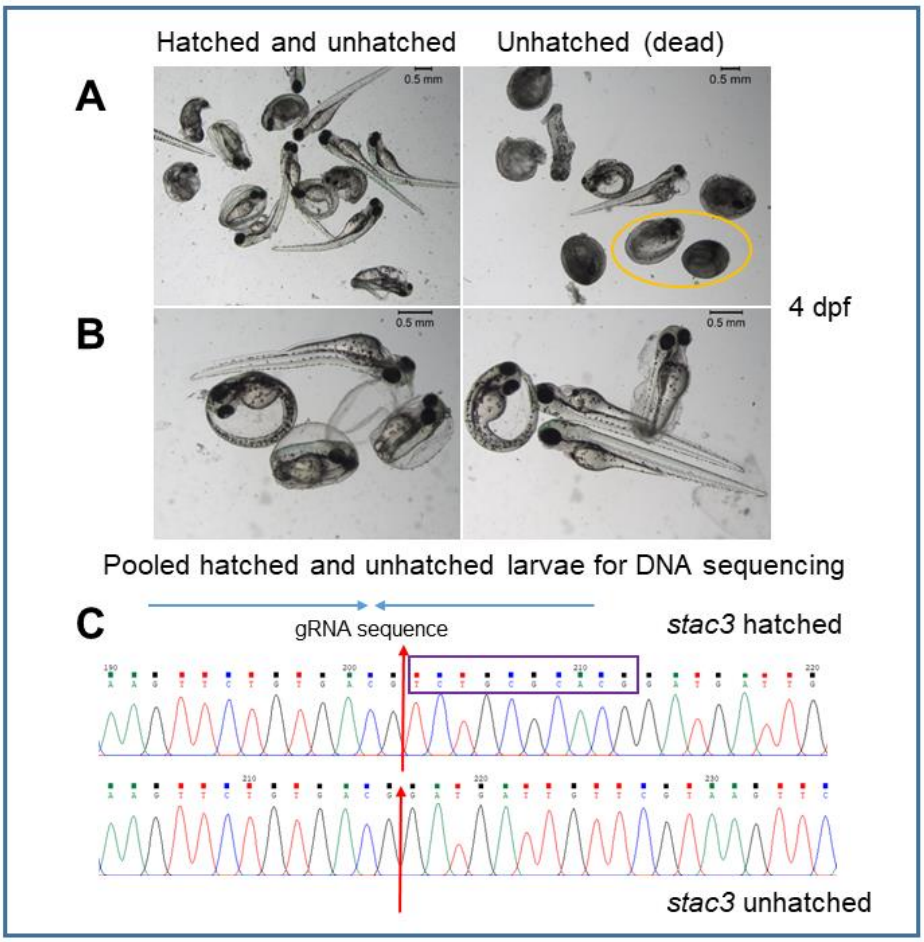

869

870 (A). Hatched and unhatched *stac3* larvae (left panel). Dead *stac3*$^{-/-}$ larvae within chorion are
871 shown in the yellow circle in the right panel. (B). Representative images of hatched and unhatched
872 *stac3* larvae (n=10) pooled for sequencing (left and right panel). (C). All hatched and unhatched
873 larvae confirmed as wild type (top), heterozygous (not shown), and knockout larvae (bottom)
874 respectively. Knockout larvae acquired a 10 bp deletion mutation, the TCTGCGCACG sequence
875 is marked by a violet box. Scale bar: 0.5 mm.

876

S3. F-actin and slow muscle myosin staining of knockout larvae

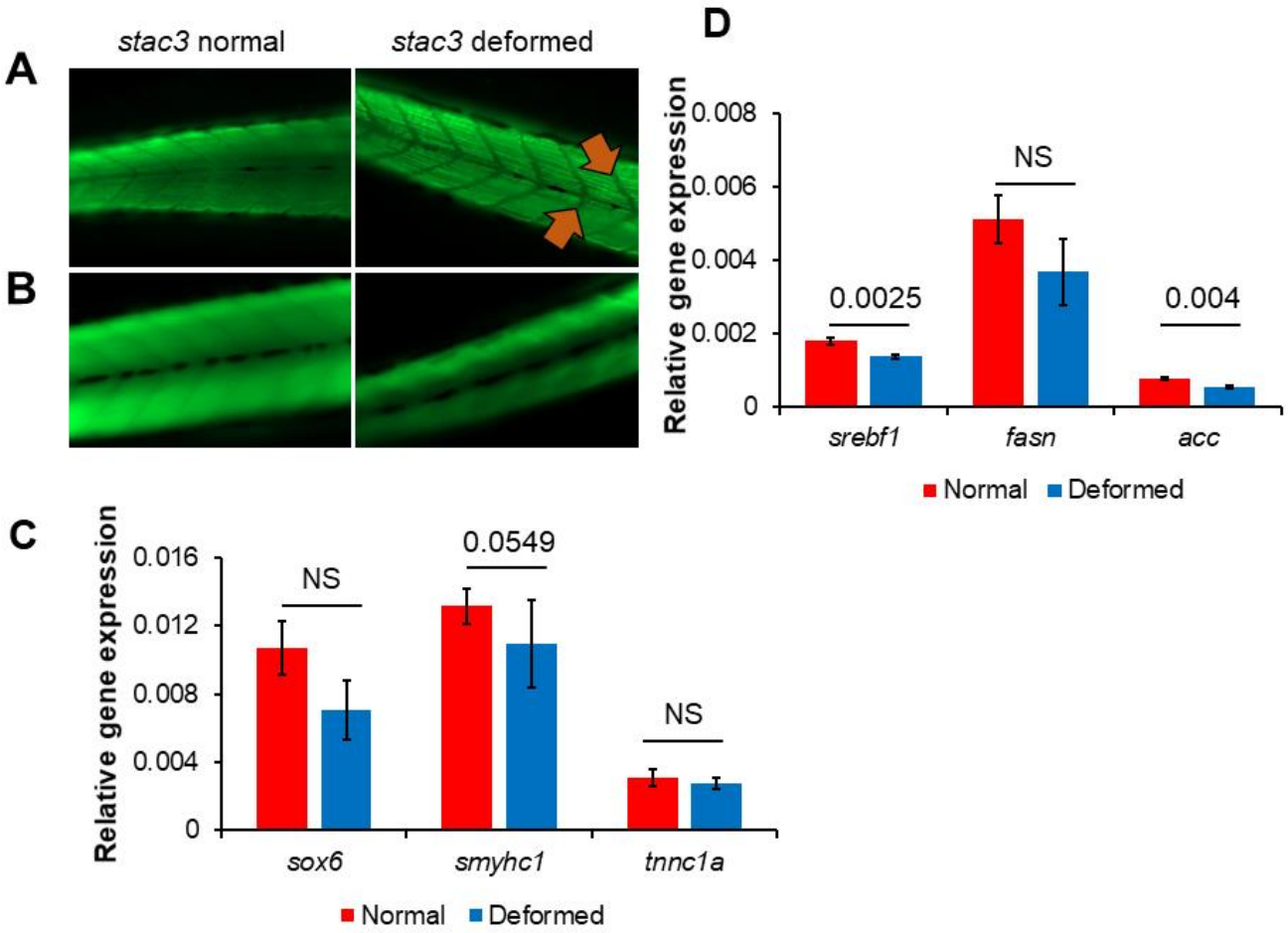

(A). Tail region of wild type and heterozygous *stac3* and *stac3* knockout larvae stained with F59 antibody. *stac3*$^{-/-}$ larvae (right) showed disorganized slow muscle fibers compared to *stac3* wild type and heterozygous siblings (left), while orange arrowheads indicate alterations in muscle fibers. (B). Reduced amounts of filamentous (F-actin) fibers were noted in whole body of *stac3* knockout larvae (right) compared to control siblings (left) stained with phalloidin and followed by '20X' magnification at 5 dpf. (C). RT-PCR analysis revealed that gene expression of skeletal muscle markers such as *sox6, smyhc1,* and *tnnca1* was unaltered, (D). whereas *srebf1* and its down-stream target acetyl co-enzyme-A were significantly down regulated, in *stac3*$^{-/-}$ larvae

887 compared to *stac3* "normal" (wild type and heterozygotes). T-Test, **p=0.0025 and p=0.004. Non-
888 significant (NS), n=10 animals for each group. Data are presented as mean ± standard deviation

889 **S4. Muscle histology of *stac3*$^{-/-}$ larvae**

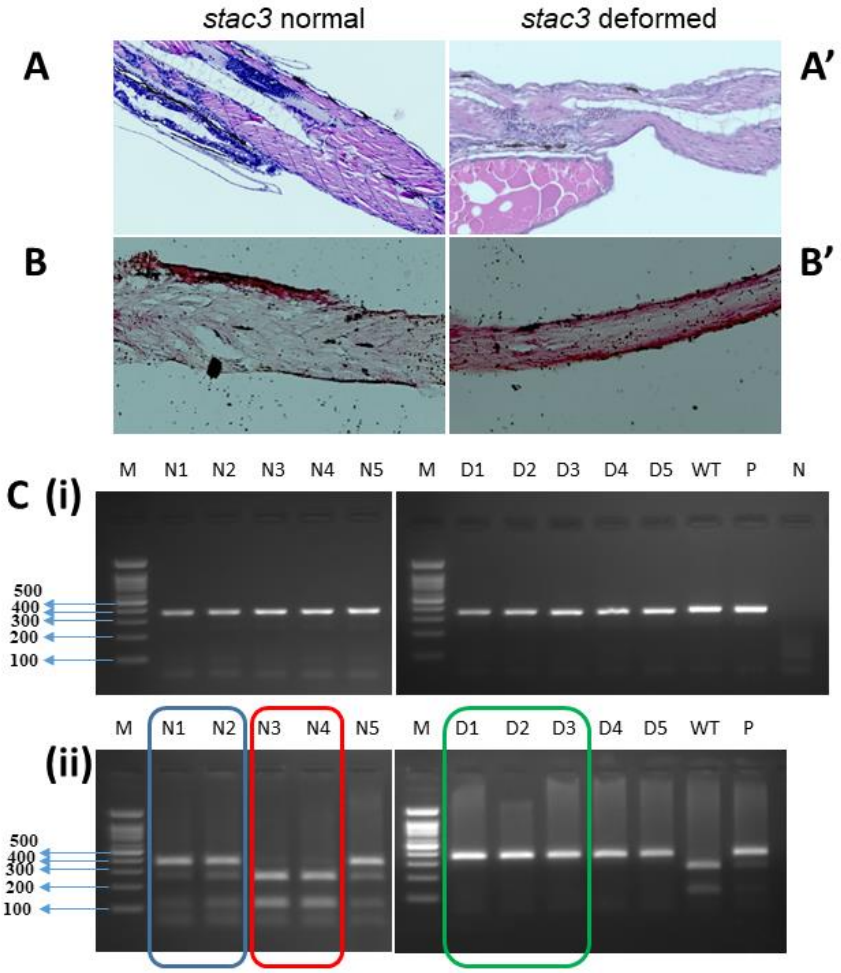

890

891 (A-A'). Paraffin based muscle sections of *stac3* wild type and heterozygous siblings and *stac3*
892 knockout larvae stained with hematoxylin showed disorganized fibers in the knockout fish (A').
893 (B-B'). OCT based muscle sections of *stac3*$^{+/+}$ and *stac3*$^{+/-}$ control siblings and knockout larvae
894 were stained with ORO dye. *stac3* knockout larvae displayed more red staining (higher lipids)
895 compared to *stac3 stac3*$^{+/+}$ and *stac3*$^{+/-}$ control siblings at 5 dpf. (D). Genotype of larvae was
896 confirmed as described in FigureS1A, B.

897

S5. Death of *stac3*$^{-/-}$ larvae at the early age

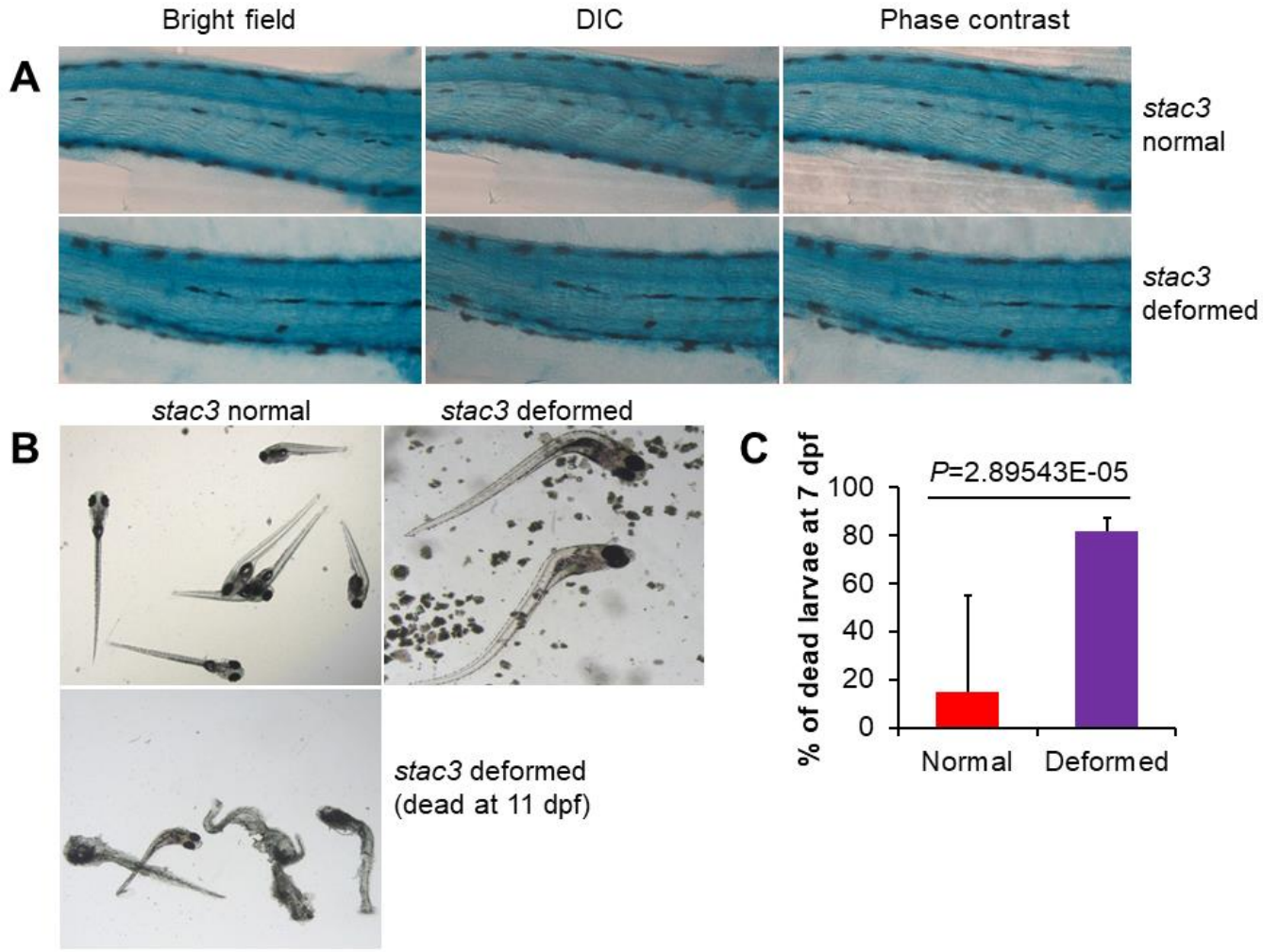

(A). Altered integrity of muscle fibers observed in *stac3* KO larvae (bottom panel) compared to *stac3* wild type and heterozygous siblings (top panel), as measured by SA-β-gal staining at 6 dpf. (B). *stac3* wild type and heterozygous siblings and KO larvae raised in an incubator confirmed that *stac3*$^{-/-}$ larvae expeditiously die by 11 dpf. *stac3* wild type and heterozygous sibling (left: top) at 9 dpf, *stac3* knockout (middle) 10 dpf, and *stac3* knockout larvae (left: bottom) 11 dpf. (C). Percentage (%) calculation of dead *stac3* knockout larvae at 7 dpf. Scale bar: 0.5-1 mm.

S6. Fasted *stac3* KO larvae show a better short-term survival

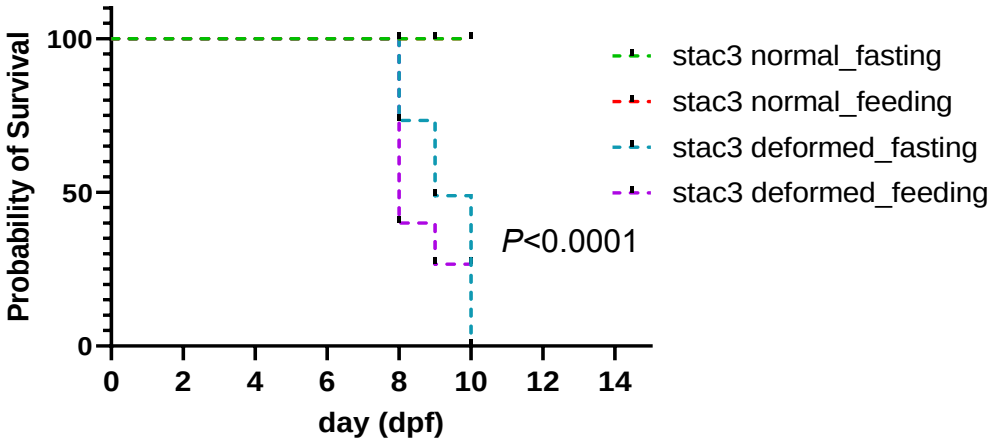

Feeding was introduced in some 7 dpf old *stac3* KO (deformed) and *stac3*$^{+/+}$ and *stac3*$^{+/-}$ (normal) control siblings. Larval growth and survival were monitored for 72 hours and the fasted and fed animals were compared. Survival percentage was calculated between fasting vs. feed *stac3* KO, *stac3*$^{+/+}$ and *stac3*$^{+/-}$ groups using Log-rank test, ****p<0.0001.

Supplementary table1. Primers used for RTqPCR

Gene name	Forward primer	Reverse primer
stac3	ATCAATAACCCGGGTCAGCA	GGCCATGATCACTCCGACTC
ryr1a	GAT GAA ACA GAG CAC ACT G	CCA CAT TTA TCC AAG CTG
myod	AACATTACAGTGGAGACTCTG	GTCATAGCTGTTCCGTCTTC
myog	GCTCCACATACTGGGGTGTC	TATAGGCGGGGACACAGTGA
myf5	TACTACAGCCTGCCGATGGA	GACTGTTGCAGTCAACCATGC
sox6	TCCACAACAAACCTCCCCTG	TTGCTGTCCGATTCCATGCG
smyhc1	GCTAACAGGCAGGCATCAGA	TGCATTTGGGAATCCTTGACA
tnnc1a	AAAAATGAGTTCCGTGCAGC	CTTCAGGGGTAGGGTTCTGG

fasn	TTCTGTAACGTTGCCGGGAG	TTCTTGAATCTGAACGCGGG
srebf1	ATGAATCTGTCTTTTGACGACACTTCT	TCAGGTGGATGTGACGGTG
rpl32	GAATCCAGAGGGCAGCATGT	GTCAAGATCAGGGCAAACTGG

Supplementary table2. Percentage (%) of dead *stac3* KO larvae at 7 dpf

Larva condition	**Age: 7 dpf**					
	exp1	**exp2**	**exp3**	**Average**	**% in total population**	**% of dead**
stac3$^{+/+}$ and *stac3*$^{+/-}$ control siblings	324	379	300	334.33	87.14	14.76
stac3$^{-/-}$ (KO)	45	47	56	49.33	12.86	81.76
stac3 dead larvae (belong to KO group)	45	47	29	40.33	10.51	
Total	369	426	356	383.67	100.00	

Supplementary table3. Muscle pathology identification by blind analysis of zebrafish larva at 6 dpf

S.NO	**Birefringence image ID**	**Bright image ID**	**Muscle pathology**	**Remarks**	**Genotype**
1	Mil_11593	Mil_11594	none	out of focus	*stac3*$^{+/-}$
2	Mil_11596	Mil_11597/9	none		*stac3*$^{+/-}$
3	Mil_11603	Mil_11604	none	out of focus	*stac3*$^{+/-}$
4	Mil_11605	Mil_11606	none	out of focus	*stac3*$^{+/+}$
5	Mil_11608	Mil_11609		very weak signal	*stac3*$^{-/-}$
6	Mil_11612	Mil_11613	patchy	very weak signal	*stac3*$^{-/-}$
7	Mil_11614	Mil_11615	patchy	very weak signal	*stac3*$^{-/-}$

8	Mil_11616	Mil_11617	"condensed"	very weak signal	*stac3*$^{-/-}$
9	Mil_11618	Mil_11619	patchy	very weak signal	*stac3*$^{-/-}$
10	Mil_11620	Mil_11621	patchy	very weak signal	*stac3*$^{-/-}$
11	Mil_11622	Mil_11623	"condensed"	very weak signal	*stac3*$^{-/-}$
12	Mil_11624	Mil_11625	patchy		*stac3*$^{-/-}$
13	Mil_11629	Mil_11630	patchy	weak signal	*stac3*$^{-/-}$
14	Mil_11631	Mil_11632	none		*stac3*$^{+/+}$
15	Mil_11633	Mil_11634	none	out of focus	*stac3*$^{+/+}$
16	Mil_11636	Mil_11637	none	out of focus	*stac3*$^{+/-}$
17	Mil_11638	Mil_11639	none	out of focus	*stac3*$^{+/-}$
18	Mil_11640	Mil_11641	none	out of focus	*stac3*$^{+/-}$
19	Mil_11642	Mil_11643	none	out of focus	*stac3*$^{+/+}$
20	Mil_11645	Mil_11646	none	out of focus	*stac3*$^{+/-}$
21	Mil_11647	Mil_11648	none	out of focus	*stac3*$^{+/-}$
22	Mil_11649	Mil_11650	none	out of focus	*not genotyped*
23	Mil_11651	Mil_11652	none		*not genotyped*
24	Mil_11655	Mil_11656	none	out of focus	*not genotyped*
25	Mil_11657	Mil_11658	none	out of focus	*not genotyped*

26	Mil_11659	Mil_11660	none		*not genotyped*
27	Mil_11661	Mil_11662	none	out of focus	*not genotyped*
28	Mil_11663	Mil_11664	patchy		*not genotyped*
29	Mil_11667	Mil_11668	patchy	very weak signal	*not genotyped*

Supplementary materials and methods

With the guide RNA targeted exon-4 sequence of *stac3* gene, we identify suitable restriction enzymes using NEB Cutter (**https://nc3.neb.com/NEBcutter/**) for genotyping zebrafish larvae, while the guide RNA sequence has a restriction digestion site at its 3 prime for genotyping.

stac3

>NM_001003505.1 Danio rerio SH3 and cysteine rich domain 3 (stac3), mRNA

CAAACTTCTGTACAAGTGTTCAATCCTCAGTTCAGAGCAGTCTGGTTATTACTGAGTTAAGATTATCTTC

TGTGCTAAAGCAAATATTAACTTATCTGTATCAGGGTCACACCTCGCTGACTGAAAACTGGGATTATAGC

ACAGAAACAGATCATCTACAGGTGCGGATTTCTGCTGACTGACTGCGTCTGAAGAGGCTGGACTGATGGC

TCAATATGACCAACTGGAGGATAAAGACTCGCTGGACATCCACGATAACCCTCCAGCGCCAGAGAATGTG

GTGAAAGAGGACGACAACACTGTGTATTTTGTGTATGATGAAGAGGTGGAGGAAGAAGAAGCTCCTCCGC

CACCCACCCCGGAGCCCATAGTCCAGGTCAATGACAAACCACACAAATTCAAGGACCACTACTGCAAGAA

ACCCAAGTTCTGTGACGTCTGCGCACGGATGATTGTTCTCAATAATAAGTTTGCGCTGCGCTGTAAAAAC

TGCAAGACCAACATCCACCACTCCTGCCAGTCATACGTGCAGTTCCAGAGATGCTTCGGCAAAATACCTC

CTGGGTTCAGACGGGCGTACAGCTCTCCTCTCTATGACCAGGAGATCAATAACCCGGGTCAGCAGAACCG

CACAGATCCGGTGTTCGACACGCTGAGAGTCGGAGTGATCATGGCCAATAAAGAGAGGAAGAAAGGCTCA

GAGGACAAGAAGAACATGATGATGATGATGATGGAGGAGGAGGAAGCTCAACAGCCCAAAGAGGATGAAG

AGGGTGCTGAGGGGAAGCAAGATGGAGACAAGAAAGACAAAACCGCAACAGATGACAAGAACAAGAAGCA

GCAGCAGACCTTCAGTCAGTCGCATTATTATATGGCTCTGTATCGCTTTAAAGCCATCGAGAAAGATGAT

CTGGACTTCCATCCAGGAGATCGTATAACTGTTTTGGATGACTCTAATGAGGAGTGGTGGAGGGGCAAGA

TTGGTGAGAAGACGGGTTATTTACCCATGACCTACATCATCCGGGTTCGAGCTGGCGAGCGGGTTTATAA

AGTGACCCGATCATTTGTGGGAAACCGAGAGATGGGCCAGATCACCCTGAAGAAAGACCAGATCGTGGTG

AAGAAAGGAGAGGAGGTGAACGGATATCTGAAGGTCAGCACTGGCCGTAAACTGGGCTTCTTCCCTGCGG

ATCTGCTGCATGAGCTCTAATAATCAGCAGACCAGCAGAAGGATGAAGAGAGACGGAGCATGCACACAGC

GGCTGCGTTACACTCCACTTTTACACACACACTCACAAACATCCCTTCACTTGTTCCCTCAGCGAAATCC

CTGCCGCTATTATGAAGTACATACCTGTTCATCAAGTGAACGAGTGAAGATTTAGATGTTGACCCTAGCT

TTTGTCAGATTTTTCAAGTCTGCTTCATATGTCTAATATATGTCCTAGAATGCGATGTGATTGTGACGTC

TCAACAGTGTAGTGCTCAAGTGCTCAAGGGTTTAGGGCACTCCATTTAAACCCATTCAGATTCTCCGCCA

GTAGTGGACACATATGTAACCTCATTAATGCTGTACATCCAAGGGAACGAGATGAAGGGAAGTTAGTGAG

TCAAGAACATAAAATATTGTACTGGAACGCAGCCCCAGTCTCATTTCAACACACAATACACTCTTCCAAA

TAAATGTGCCATGAAGAGCCAAAAAAAAAAAAAAAAAAAAAAA

gRNA

AGTTCTGTGACGTCTGCGCA

***stac3* exon 4**

tttgcattcactaacattaactaatggactattattgagtagtgttttcaacgttagttctgctggggcttcataaatgagacctgcagtgtgta

cggtgagcacacagccgactcggtcatcctctcaggtgtattttctcatcctcagGTGTATTTTGTGTATGATGAAGAGG

TGGAGGAAGAAGAAGCTCCTCCGCCACCCACCCCGGAGCCCATAGTCCAGGTCAACGAC

AAACCACACAAATTCAAGGACCACTACTGCAAGAAACCCAAGTTCTGTGACGTCTGCGCACC

GGATGATTGTTCgtaagttcacattgatagcaagttacaataacagcacacatattgtctcaacccttgcctcatatgtttgcatt

gttaaggtaaactgttcttgccaaaatgaatgatcagatacacacataagttgcagaagaaactctacgatatgaaacgtatgcgctgt

gtggtgtctctactttcag

FspI restriction enzyme

5'...T G C▾G C A... 3'

3'...A C G▴C G T... 5'

967 Pcr product 363bp

968 After cut 247bp 113bp

969 Genotyping of *stac3*$^{-/-}$ vs. *stac3*$^{+/+}$ and *stac3*$^{+/-}$ control siblings was confirmed as described in
970 FigureS1A, B. Blue: coding region, green color marks the gRNA region in exon4 of the *stac3* gene
971 and protospacer adjacent motif sequence is in yellow, while red denotes restriction digestion site.

972